Article

Preparation and Characterization of π-Stacking Quinodimethane Oligothiophenes. Predicting Semiconductor Behavior and Bandwidths from Crystal Structures and Molecular Orbital Calculations

Daron E. Janzen, Michael W. Burand, Paul C. Ewbank, Ted M. Pappenfus, Hiroyuki Higuchi, Demetrio A. da Silva Filho, Victor G. Young, Jean-Luc Brdas, and Kent R. Mann

J. Am. Chem. Soc., **2004**, 126 (46), 15295-15308• DOI: 10.1021/ja0484597 • Publication Date (Web): 28 October 2004

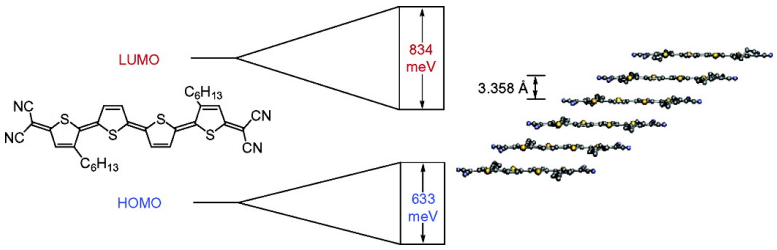

More About This Article

Additional resources and features associated with this article are available within the HTML version:

- Supporting Information
- Links to the 5 articles that cite this article, as of the time of this article download
- Access to high resolution figures
- Links to articles and content related to this article
- Copyright permission to reproduce figures and/or text from this article

View the Full Text HTML

J|A|C|S
ARTICLES
Published on Web 10/28/2004

Preparation and Characterization of π-Stacking Quinodimethane Oligothiophenes. Predicting Semiconductor Behavior and Bandwidths from Crystal Structures and Molecular Orbital Calculations

Daron E. Janzen,[†] Michael W. Burand,[†] Paul C. Ewbank,[†] Ted M. Pappenfus,[†] Hiroyuki Higuchi,[‡] Demetrio A. da Silva Filho,[§] Victor G. Young,[†] Jean-Luc Brédas,[§] and Kent R. Mann*,[†]

Contribution from the Department of Chemistry, University of Minnesota, Minneapolis, Minnesota 55455, Department of Chemistry, Toyama University, Toyama 930-8555, Japan, and School of Chemistry and Biochemistry, Georgia Institute of Technology, Atlanta, Georgia 30332

Received March 17, 2004; E-mail: mann@chem.umn.edu

Abstract: A series of new quinodimethane-substituted terthiophene and quaterthiophene oligomers has been investigated for comparison with a previously studied quinoid oligothiophene that has demonstrated high mobilities and ambipolar transport behavior in thin-film transistor devices. Each new quinoidal thiophene derivative shows a reversible one-electron oxidation between 0.85 and 1.32 V, a quasi-reversible one-electron second oxidation between 1.37 and 1.96 V, and a reversible two-electron reduction between −0.05 and −0.23 V. The solution UV−vis−NIR spectrum of each compound is dominated by an intense ($\epsilon \cong$ 100 000 M^{-1} cm^{-1}) low energy $\pi-\pi^*$ transition that has a λ_{max} ranging between 648 and 790 nm. All X-ray crystal structures exhibit very planar quinoidal backbones and short intermolecular π-stacking distances (3.335−3.492 Å). Structures exhibit a single π-stacking distance with parallel cofacial stacking (sulfur atoms of equivalent rings pointed in the same direction) or with alternating distances and antiparallel cofacial stacking (sulfur atoms of equivalent rings pointed in the opposite direction). Examples of the layered and herringbone-packing motifs are observed for both the parallel and the antiparallel cofacial stacking. Analysis of the X-ray structures and molecular orbital calculations indicates that all of these compounds have one-dimensional electronic band structures as a result of the π-stacking. For structures with a unique π-stacking distance, a simple geometric overlap parameter calculated from the shape of the molecule and the slip from perfect registry in the π-stack correlates well with the transfer integrals (t) calculated using molecular orbital theory. The calculated valence (633 meV) and conduction (834 meV) bandwidths for a quinoid quaterthiophene structure are similar to those calculated for the benchmark pentacene and indicate that both hole and electron mobilities could be significant.

Introduction

Polymeric and oligomeric materials have shown excellent promise for use in organic electronic devices such as thin-film field effect transistors (FETs) and light-emitting diodes (LEDs).[1] Soluble organic semiconducting electronic materials have potential advantages over existing inorganic semiconductors including processability and tunable electronic properties. Organic electronic materials are suitable for large area device manufacture via printing[2] because of mechanical flexibility and economical manufacture. If the proper "soft" materials can be discovered, processing techniques requiring expensive clean room and highly specialized lithographic tools could be eliminated in many applications.

The inherent electronic and optical properties of these materials derive from the extended π-system. Molecular structure, conformation, and the degree of overlap between molecules determine the nature and magnitude of the semiconductor properties. In general, the mechanism of charge transport[3] in these well-ordered soft materials can be summarized as bandlike at lower temperatures, where the mobility is primarily determined by the valence and conduction bandwidths, and thermally activated localized polaronic hopping at higher temperatures, where geometry relaxation (vibrational) effects play a major role. P-channel,[4−6] n-channel,[7−11] and, most recently, ambipolar[11] materials that can function as both have been described.

The preeminent (and somewhat enigmatic) organic p-channel semiconducting material is pentacene. Pentacene and related oligoacenes exhibit some of the highest carrier mobilities measured in FET devices to date, even though the herringbone 2-D edge-to-face layered structure does not contain π-stacks.[4] The critical edge-to-face interactions that produce the electronic

[†] University of Minnesota.
[‡] Toyama University.
[§] Georgia Institute of Technology.

(1) (a) Dimitrakopoulos, C. D.; Malenfant, P. R. L. *Adv. Mater*. **2002**, *14*, 99−117. (b) *Handbook of Oligo- and Polythiophenes*; Fichou, D., Ed.; Wiley-VCH: Weinheim, Germany, 1999.

(2) (a) Blanchet, G.; Rogers, J. *J. Imaging Sci. Technol*. **2003**, *47*, 296−303. (b) Blanchet, G. B.; Loo, Y.-L.; Rogers, J. A.; Gao, F.; Fincher, C. R. *Appl. Phys. Lett*. **2003**, *82*, 463−465.

(3) (a) Karl, N. *Synth. Met*. **2003**, *133*−*134*, 649−657. (b) Campbell, I. H.; Smith, D. L. *Int. J. High Speed Electron. Syst*. **2001**, *11*, 585−615.

10.1021/ja0484597 CCC: $27.50

properties of pentacene are apparently diminished by any attempts at functionalization. In the extreme, substitution causes transformation to a π-stacked structure.[12] Derivatization is necessarily accomplished at the edges of pentacene molecules, disrupting the edge-to-face overlap. In contrast, molecules that π-stack are more flexible. Substituents can be accommodated by slippage, rotation, or expansion along the stacking axis while maintaining some measure of intermolecular overlap.[13] As the π-overlap at perfect alignment can be large, even relatively large deviations from perfect registry can in principle still give materials with appreciable mobilities.

As it is a commonly held belief that strong intermolecular interactions (such as π-stacking) can give materials with high charge mobilities, many polymeric and oligomeric thiophene systems have been investigated and found to be good p-channel materials. For example, p-channel FETs constructed with defect-free head-to-tail regioregular poly(3-hexylthiophene) (HT-P3HT) (96% regioregularity) have shown excellent mobilities of 0.05−0.1 $cm^2/(V\ s)$.[5] The percent regioregularity and the method of film deposition (cast vs spun) also affect the orientation of the layered lamellae with respect to the substrate. The measured mobility was highly anisotropic, with the mobility in the π-stacking direction better by more than a factor of 100.

Because it can be difficult to determine X-ray structures of amorphous or semicrystalline polymers such as HT-P3HT, the study of well-characterized oligomeric systems should help establish detailed structure−property relationships. A recent example is bisdithienothiophene (BDT), a molecule with a short π-stacking distance of 3.557 Å and good π-overlap.[6] Calculations[14] indicate BDT has significant interchain transfer integrals (t) for both the HOMO and the LUMO (172 and 27 meV, respectively), giving valence and conduction bandwidths ($4t$) of 688 and 108 meV, respectively. The p-channel FET devices constructed with BDT[6] have mobilities of 0.02−0.05 $cm^2/(V\ s)$, which lie within 2 orders of magnitude of the best pentacene devices. Thus, both polymeric and oligomeric thiophenes are viable alternatives to pentacene for p-channel materials and will also offer the chance of property modification by derivatization.

Although thiophene derivatives are less studied as n-channel materials,[7] where intermolecular overlap is equally critical, the *N*,*N*′-dialkylated 3,4,9,10-perylenetetracarboxylic acid diimides (PTCDIs) are a particularly well-studied family of π-stacking n-channel materials.[8] Devices with mobilities as high as 0.6 $cm^2/(V\ s)$ have been constructed using octyl disubstituted PTCDI (C8PTCDI).[9] Furthermore, it has been shown that an important electronic property (the HOMO−LUMO optical band gap) correlates with simple crystal packing parameters.[13] Similar correlations have not been described for quinoidal oligothiophenes, and only recently have the geometric factors been delineated for aromatic oligothiophenes.[15]

With these (and many other excellent studies as a backdrop), we seek structural correlations for the observed properties of the quinoidal oligothiophene **DCMT** (3′,4′-dibutyl-5,5″-bis(dicyanomethylene)-5,5″-dihydro-2,2′:5′,2″-terthiophene).[10,11,16,17] This family of molecules may be described electronically as oxidized oligothiophene dications stabilized by malononitrile anion capping groups. A spectroscopic comparison of **DCMT** and its reduced forms with the corresponding aromatic oligothiophene and its oxidized forms confirms that the π-systems are equivalent.[16] Previously, we reported that vapor- and solution-deposited films of **DCMT** function as n-channel semiconductors with electron mobilities of 0.005 and 0.002 $cm^2/(V\ s)$, respectively.[10] More recently, devices constructed from **DCMT** with different film morphologies demonstrate either enhanced n-channel mobilities (0.2 $cm^2/(V\ s)$) or ambipolar (n-channel and p-channel depending on the sign of the gate bias) behavior with lower mobilities (both hole and electron mobilities $< 10^{-4}$ $cm^2/(V\ s)$).[11] The unique electronic structure of the quinoid thiophene molecules allows them to function as simultaneous donors and acceptors. Their strong propensity to π-stack and the availability of soluble *n*-hexyl-substituted precursor oligomers make them ideal for systematic study of how the solid-state structure affects semiconductor performance. This work represents our efforts to further understand the effects of alkyl substitution and oligomer length on the molecular and solid-state properties of quinoidal oligothiophenes (Figure 1). Analyzing the relationships between packing structure and solid-state electronic structure can provide insight into the choice and design of materials for good FET performance.

Experimental Section

General Considerations. All syntheses were carried out under an inert atmosphere of Ar or N_2. 1,2-Dimethoxyethane and *N*,*N*-dimethylformamide were distilled from Na/benzophenone under N_2; CH_2Cl_2 was distilled from CaH_2 under N_2. $Pd(PPh_3)_4$ (Strem Chemicals, Inc.), malononitrile (Acros Organics), *N*-iodosuccinimide, 3-hexylthiophene, 2,5-dibromothiophene, and 5,5′-dibromo-2,2′-bithiophene (Aldrich) were used as received as were other reagents unless otherwise indicated. 2-Bromo-3-hexylthiophene was synthesized according to literature

(4) (a) Campbell, R. B.; Robertson, J. M.; Trotter, J. *Acta Crystallogr.* **1961**, *14*, 705−711. (b) Lin, Y. Y.; Gundlach, D. J.; Nelson, S. F.; Jackson, T. N. *IEEE Electron Device Lett.* **1997**, *18*, 606−608. (c) Butko, V. Y.; Chi, X.; Lang, D. V.; Ramirez, A. P. *Appl. Phys. Lett.* **2003**, *83*, 4773−4775. (d) Meng, H.; Bendikov, M.; Mitchell, G.; Helgeson, R.; Wudl, F.; Bao, Z.; Siegrist, T.; Kloc, C.; Chem, C.-H. *Adv. Mater.* **2003**, *15*, 1090−1093. (e) Butko, V. Y.; Chi, X.; Ramirez, A. P. *Solid State Commun.* **2003**, *128*, 431−434.

(5) Sirringhaus, H.; Brown, P. J.; Friend, R. H.; Nielsen, M. M.; Bechgaard, K.; Langeveld-Voss, B. M. W.; Spiering, A. J. H.; Janssen, R. A. J.; Meijer, E. W.; Herwig, P.; de Leeuw, D. M. *Nature* **1999**, *401*, 685−688.

(6) Li, X.-C.; Sirringhaus, H.; Garnier, F.; Holmes, A. B.; Moratti, S. C.; Feeder, N.; Clegg, W.; Teat, S. J.; Friend, R. H. *J. Am. Chem. Soc.* **1998**, *120*, 2206−2207.

(7) (a) Facchetti, A.; Yoon, M.-H.; Stern, C. L.; Katz, H. E.; Marks, T. J. *Angew. Chem., Int. Ed.* **2003**, *42*, 3900−3903. (b) Facchetti, A.; Mushrush, M.; Katz, H. E.; Marks, T. J. *Adv. Mater.* **2003**, *12*, 33−38. (c) Sakamoto, Y.; Komatsu, S.; Suzuki, T. *J. Am. Chem. Soc.* **2001**, *123*, 4643−4644. (d) Yassar, A.; Demanze, F.; Jaafari, A.; El Idrissi, M.; Coupry, C. *Adv. Funct. Mater.* **2002**, *12*, 699−708.

(8) Struijk, C. W.; Sieval, A. B.; Dakhorst, J. E. J.; van Dijk, M.; Kimkes, P.; Koehorst, R. B. M.; Donker, H.; Schaafsma, T. J.; Picken, S. J.; van der Craats, A. M.; Warman, J. M.; Zuilhof, H.; Sudholter, E. J. R. *J. Am. Chem. Soc.* **2000**, *122*, 11057−11066.

(9) Malenfant, P. R.; Dimitrakopoulos, C. D.; Gelorme, J. D.; Kosbar, L. L.; Graham, T. O.; Curioni, A.; Andreoni, W. *Appl. Phys. Lett.* **2002**, *80*, 2517−2519.

(10) Pappenfus, T. M.; Chesterfield, R. J.; Frisbie, C. D.; Mann, K. R.; Casado, J.; Raff, J. D.; Miller, L. L. *J. Am. Chem. Soc.* **2002**, *124*, 4184−4185.

(11) Chesterfield, R. J.; Newman, C. R.; Pappenfus, T. M.; Ewbank, P. C.; Haukaas, M. H.; Mann, K. R.; Miller, L. L.; Frisbie, C. D. *Adv. Mater.* **2003**, *15*, 1278−1282.

(12) Haddon, R. C.; Chi, X.; Itkis, M. E.; Anthony, J. E.; Eaton, D. L.; Siegrist, T.; Mattheus, C. C.; Palstra, T. T. M. *J. Phys. Chem. B* **2002**, *106*, 8288−8292.

(13) Klebe, G.; Graser, F.; Hadicke, E.; Berndt, J. *Acta Crystallogr.* **1989**, *B45*, 69−77.

(14) Cornil, J.; Beljonne, D.; Calbert, J.-P.; Bredas, J.-L. *Adv. Mater.* **2001**, *13*, 1053−1067.

(15) Curtis, M. D.; Cao, J.; Kampf, J. W. *J. Am. Chem Soc.* **2004**, *126*, 4318−4328.

(16) Pappenfus, T. M.; Raff, J. D.; Hukkanen, E. J.; Burney, J. R.; Casado, J.; Drew, S. M.; Miller, L. L.; Mann, K. R. *J. Org. Chem.* **2002**, *67*, 6015−6024.

(17) Casado, J.; Miller, L. L.; Mann, K. R.; Pappenfus, T. M.; Higuchi, H.; Orti, E.; Milian, B.; Pou-Amerigo, R.; Hernandez, V.; Lopez Navarrete, J. T. *J. Am. Chem. Soc.* **2002**, *124*, 12380−12388.

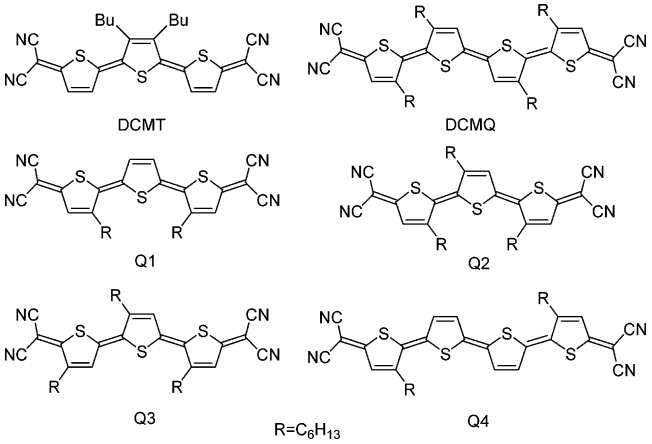

Figure 1. Molecular structures of quinoidal terthiophenes.

procedures.[18] 5,5‴-Bis(dicyanomethylene)-3,3′,4″,3‴-tetrahexyl-5,5‴-dihydro-2,2′:5′,2″:5″,2‴-quaterthiophene (**DCMQ**) was synthesized by a previously reported method.[18] Malononitrile was purified by vacuum distillation prior to use for the synthesis of **Q3**. ^{1}H NMR spectra were measured on a Varian Unity 300 (300 MHz) or Varian Inova 300 (300 MHz) instrument. The chemical shifts are reported in ppm, and the coupling constants (*J*) are given in Hz. All spectra are referenced to the residual proton peak of the solvent: chloroform, 7.27 ppm; dichloromethane, 5.32 ppm; and 1,1,2,2-tetrachloroethane, 6.00 ppm; for ^{13}C spectra, the reference is the chloroform peak at 77.23 ppm. Mass spectra were obtained on a Finnigan MAT 95 or VG 7070E-HF mass spectrometer. Fast-atom bombardment (FAB) MS were acquired with a *m*-nitrobenzyl alcohol/trifluoroacetic acid matrix. Elemental analyses were obtained from Quantitative Technologies Inc., Whitehouse, NJ. Solution electronic spectra in dichloromethane solutions were collected on a computer-controlled Cary 17 or Ocean Optics spectrophotometer. Electrochemical experiments were performed with a BAS 100B electrochemical analyzer and a glassy carbon working electrode. Solutions of electroactive compound (∼0.5 mM) were made in dichloromethane with 0.1 M $TBAPF_6$ as the supporting electrolyte. Potentials are reported versus aqueous Ag/AgCl and are not corrected for the junction potential. The $E^{\circ\prime}$ value for the ferrocenium/ferrocene couple under the conditions used in this study was +0.42 V.[19]

2-Chloro-3-hexylthiophene (A). Compound **A** was synthesized by a slight modification of a previously reported method[20] for the 3-octylthiophene analogue. Separation of starting material, desired product, and the dichlorinated byproduct (**B**) was difficult to accomplish by distillation. Thus, an excess of chlorinating agent was employed to ensure that no 3-hexylthiophene remained in the product. The small amount of dichlorinated byproduct (**A**:**B** ratio = 5:1) formed using this strategy was inert to subsequent reactions and could be removed at a later stage. The colorless oil was distilled at 60 °C, 0.15 Torr. ^{1}H NMR (300 MHz, $CDCl_3$): δ 7.02 (d, 1H, J = 8.4), 6.80 (d, 1H, J = 8.4), 2.57 (t, 2H), 1.57 (t, 2H), 1.31 (m, 6H), 0.89 (t, 3H).

2,5-Dichloro-3-hexylthiophene (B). Compound **B** was observed as a byproduct in the synthesis of **A** (above). ^{1}H NMR (300 MHz, $CDCl_3$): δ 6.65 (s, 1H), 2.51 (t, 2H), 1.57 (m, 2H), 1.31 (m, 6H), 0.89 (t, 3H).

2-Chloro-3-hexyl-5-iodothiophene (C). Compound **C** was synthesized by a slight modification of a previously reported method[20] for the 3-octylthiophene analogue. The starting material was the 5:1 mixture of **A** and **B** reported above. The product obtained was a 5:1 mixture of **C** and **B**, recovered as a colorless oil by Kugelrohr distillation at 95 °C, 0.016 Torr. ^{1}H NMR (300 MHz, $CDCl_3$): δ 6.97 (s, 1H), 2.52 (t, 2H), 1.54 (t, 2H), 1.30 (m, 6H), 0.88 (t, 3H).

5,5-Dimethyl-2-(3-hexyl-2-thienyl)-1,3,2-dioxaborinane (D). Compound **D** was synthesized from 2-bromo-3-hexylthiophene by the reported method[20] for the 3-octylthiophene analogue. **D** was obtained as a colorless oil (6.59 g, 23.5 mmol, 67%). ^{1}H NMR (300 MHz, $CDCl_3$): δ 7.44 (d, 1H, J = 4.8), 7.01 (d, 1H, J = 4.8), 3.77 (s, 4H), 2.89 (t, 2H), 1.59 (m, 2H), 1.33 (m, 6H), 1.04 (s, 9H), 0.90 (t, 3H). HREIMS $C_{15}H_{25}BO_2S$ calcd, 280.1668; found, 280.1670 (M^+).

3,4′-Dihexyl-5′-chloro-2,2′-bithiophene (E). Compound **E** was synthesized by a previously reported method[20] for the 3-octylthiophene analogue from the starting materials **D** (3.196 g, 11.40 mmol) and a 4:1 mixture of **C** (4.03 g, 9.81 mmol) and **B**. The crude product was dissolved in hexanes and filtered through a short pad of silica to remove unreacted **D** and phosphanes (catalyst ligands). The filtrate was concentrated, and the low-boiling components (including residual **B** and **C**) were removed by Kugelrohr distillation (95 °C, 0.07 Torr) to leave a yellow oil (3.39 g, 94%) that was sufficiently pure for subsequent reaction. ^{1}H NMR (300 MHz, $CDCl_3$): δ 7.19 (d, 1H, J = 5.1), 6.94 (d, 1H, J = 5.1), 6.83 (s, 1H), 2.74 (t, 2H), 2.61 (t, 2H), 1.65 (t, b, 4H), 1.37 (m, 12H), 0.93 (m, 6H). ^{13}C NMR (300 MHz, $CDCl_3$): δ 139.8, 139.5, 132.5, 129.9, 126.5, 123.8, 31.6 (two peaks separated by 0.02 ppm), 30.7, 29.5, 29.2, 29.1, 28.9, 28.0, 22.6, 14.1.

5′-Chloro-5-iodo-3,4′-dihexyl-2,2′-bithiophene (F). Compound **F** was synthesized from **E** in 59% yield by a previously reported method[20] for the 3-octylthiophene analogue. ^{1}H NMR (300 MHz, $CDCl_3$): δ 7.06 (s, H), 6.75 (s, H), 2.66 (t, 2H), 2.57 (t, 2H), 1.58 (m, 4H), 1.33 (m, 12H), 0.90 (m, 6H). ^{13}C NMR (300 MHz, $CDCl_3$): δ 141.9, 139.9, 138.7, 136.2, 131.3, 127.2, 124.9, 72.0, 31.8, 30.8, 29.7, 29.3, 29.1, 28.2, 22.8, 14.3 (two peaks separated by 0.02 ppm). HREIMS $C_{20}H_{28}ClIS_2$ calcd, 494.0366; found, 494.0334 (M^+).

5-Chloro-3′,3″,4-trihexyl-2,2′:5′,2‴-terthiophene (G). Compound **G** was synthesized from **F** in 38% yield by a previously reported method[20] for the 3-octylthiophene analogue. ^{1}H NMR (300 MHz, $CDCl_3$): δ 7.17 (d, 1H, J = 5.4), 6.93 (d, 1H, J = 5.4), 6.93 (s, 1H), 6.82 (s, 1H), 2.78 (t, 2H), 2.71 (t, 2H), 2.58 (t, 2H), 1.64 (m, 6H), 1.33 (m, 18H), 0.91 (m, 9H). HREIMS $C_{30}H_{43}ClS_3$ calcd, 534.2215; found, 534.2179 (M^+).

2,5-Dibromo-3-hexylthiophene (H). This compound has been previously prepared by a different procedure.[18] In the dark, *N*-bromosuccinimide (1.38 g, 7.76 mmol) was added in portions to 2-bromo-3-hexylthiophene (1.92 g, 7.76 mmol) in a solution of chloroform and acetic acid (80 mL, 1:1 v/v) at 0 °C. The mixture was allowed to warm to room temperature and stirred for 24 h. Water (50 mL) was added, and the organic layer was extracted with chloroform, washed with 2.0 M KOH (2 × 200 mL), and dried with $MgSO_4$. ^{1}H NMR spectroscopy of the resulting oil revealed the reaction was incomplete, so the oil was redissolved in chloroform and acetic acid (80 mL, 1:1 v/v) and additional *N*-bromosuccinimide (1.08 g, 6.07 mmol) was added. The mixture was refluxed for 1.5 h. Water (100 mL) was added, and the organic layer was extracted with chloroform, washed with 2.0 M KOH (2 × 200 mL), and dried with $MgSO_4$. The solvent was removed via rotary evaporation, and the resulting dark oil was filtered through a short pad of silica with hexanes. Removal of the solvent by rotary evaporation yielded 2.21 g (87%) of **H** as a colorless oil. ^{1}H NMR (300 MHz, $CDCl_3$): δ 6.79 (s), 2.51 (t, J = 7.5), 1.56 (m), 1.30 (m), 0.90 (m).

3,3″-Dihexyl-2,2′:5′,2″-terthiophene (1).[21] Mg turnings (1.33 g, 54.8 mmol) were suspended in 50 mL of diethyl ether. A solution of 2-bromo-3-hexylthiophene (10.3 g, 41.8 mmol) in 30 mL of diethyl ether was added slowly to the reaction vessel via an addition funnel over the course of 20 min. The resulting mixture was refluxed for 1.3 h. The solution was cannulated into an addition funnel connected to a

(18) Higuchi, H.; Nakayama, T.; Koyama, H.; Ojima, J.; Wada, T.; Sasabe, H. *Bull. Chem. Soc. Jpn.* **1995**, *68*, 2363−2377.
(19) Graf, D. D.; Duan, R. G.; Campbell, J. P.; Miller, L. L.; Mann, K. R. *J. Am. Chem. Soc.* **1997**, *119*, 5888−5899.
(20) Bidan, G.; De Nicola, A.; Enee, V.; Guillerez, S. *Chem. Mater.* **1998**, *10*, 1052−1058.
(21) Gallazzi, M. C.; Castellani, L.; Zerbi, G.; Sozzani, P. *Synth. Met.* **1991**, *41*, 495−498.

second flask, which contained a solution of 2,5-dibromothiophene (3.48 g, 14.4 mmol) and Ni(dppp)Cl_2 (98 mg, 0.18 mmol) in 50 mL of diethyl ether. After slow addition of the Grignard solution via an addition funnel, the solution was refluxed for 1.25 h. The solution was cooled to 0 °C, and 1 M HCl (50 mL) was added slowly. The organic layer was extracted with diethyl ether (2 × 60 mL), washed with saturated aqueous Na_2CO_3 (200 mL), and dried with $MgSO_4$. The solvent was removed via rotary evaporation to yield a brown oil which was filtered through a short pad of silica, and then Kugelrohr distilled (203 °C, 1.5 Torr) to yield 5.66 g (94%) of **1** as a yellow oil. ^{1}H NMR (300 MHz, $CDCl_3$): δ 7.19 (d, 2H, J = 5.1), 7.06 (s, 2H), 6.95 (d, 2H, J = 5.4), 2.79 (t, J = 7.8), 1.66 (m), 1.33 (m), 0.89 (m). HREIMS $C_{24}H_{32}S_3$ calcd, 416.1666; found, 416.1668 (M^+).

3,3′,3″-Trihexyl-2,2′:5′,2″-terthiophene (2).[18,22] Compound **2** was prepared by two different methods.

Method A. A previously reported synthesis was followed;[18] the only change was that a 10-fold mol excess of 2-bromo-3-hexylthiophene was used for the coupling reaction. The yield was 85%.

Method B. Mg turnings (740 mg, 30.4 mmol) were suspended in 50 mL of diethyl ether. A solution of 2-bromo-3-hexylthiophene (5.75 g, 23.3 mmol) in 30 mL of diethyl ether was added slowly to the reaction vessel via an addition funnel over the course of 50 min. The resulting mixture was refluxed for 2 h. The solution was cannulated to an addition funnel connected to a second flask, which contained a solution of 2,5-dibromo-3-hexylthiophene (2.62 g, 8.02 mmol) and Ni(dppp)Cl_2 (55 mg, 0.10 mmol) in 50 mL diethyl ether. After slow addition of the Grignard solution via addition funnel, the solution was refluxed for 45 h. The solution was cooled to 0 °C, and 1 M HCl (30 mL) was added slowly, followed by the addition of water (30 mL). The organic layer was extracted with diethyl ether (3 × 50 mL), washed with saturated aqueous Na_2CO_3 (200 mL), and dried with $MgSO_4$. The solvent was removed via rotary evaporation to yield a brown oil, which was filtered through a short pad of silica, and the lower-mass impurities were removed by Kugelrohr vacuum distillation at 200 °C to yield 2.42 g (60%) of **2** as a yellow oil. ^{1}H NMR (300 MHz, $CDCl_3$): δ 7.31 (d, 1H, J = 5.1), 7.16 (d, 1H, J = 4.8), 6.98 (s, 1H), 6.98 (d, 1H, J = 4.8), 6.93 (d, 1H, J = 5.1), 2.78 (t, J = 8.1), 2.53 (m), 1.56 (m), 1.26 (m), 0.86 (m).

3,4′,4″-Trihexyl-2,2′:5′,2″-terthiophene (3).[22] A solution of **G** (1.00 g, 1.86 mmol) in 20 mL of THF under Ar was cooled to −78 °C, and *n*-butyllithium (2.5 M in hexanes, 1.49 mL, 3.73 mmol) was added dropwise over the course of 10 min. The solution was allowed to warm to 0 °C, was quenched slowly with water (25 mL), and then hexanes (25 mL) was added. After warming to room temperature, the organic phase was washed with water (3 × 30 mL) and dried with $MgSO_4$. Rotary evaporation of the solvent yielded 750 mg (80%) of **3** as a yellow oil. ^{1}H NMR (300 MHz, $CDCl_3$): δ 7.16 (d, 1H, J = 5.1), 6.97 (d, 1H, J = 1.2), 6.93 (s, 1H), 6.93 (d, 1H, J = 5.4), 6.90 (d, 1H, J = 1.5), 2.75 (m), 2.62 (m), 1.65 (m), 1.33 (m), 0.89 (m). HREIMS $C_{30}H_{44}S_3$ calcd, 500.2605; found, 500.2605 (M^+).

3,3‴-Dihexyl-2,2′:5′,2″:5″,2‴-quaterthiophene (4).[23] **4** was synthesized in a manner similar to a literature procedure[23] with the following exceptions: a slight excess of Mg (1.3 equiv) was used, reaction times were extended (31.5 h), and the product **4** was not purified by column chromatography prior to use in the next synthesis. ^{1}H NMR (300 MHz, $CDCl_3$): δ 7.19 (d, 2H, J = 5.1), 7.14 (d, 2H, J = 3.9), 7.03 (d, 2H, J = 3.6), 6.95 (d, 2H, J = 5.4), 2.79 (t, J = 7.8), 1.66 (m), 1.33 (m), 0.90 (m).

3,3″-Dihexyl-5,5″-diiodo-2,2′:5′,2″-terthiophene (1I).[24] A solution of 3,3″-dihexyl-2,2′:5′,2″-terthiophene (1.50 g, 3.60 mmol) in 60 mL of dichloromethane was cooled to 0 °C, and *N*-iodosuccinimide (1.78 g, 7.92 mmol) was added. Glacial acetic acid (1.35 mL, 23.8 mmol) was slowly added dropwise via syringe. The ice bath was removed, and the reaction mixture was allowed to stir at room temperature in the dark. After 1 h, the solution was washed with saturated aqueous Na_2CO_3 (2 × 50 mL) and dried with $MgSO_4$. The solvent was removed by rotary evaporation, and the resulting oil was purified using column chromatography (silica gel/100% hexanes) to provide 1.38 g (57%) of **1I** as a bright yellow solid. ^{1}H NMR (300 MHz, $CDCl_3$): δ 7.08 (s, 2H), 6.99 (s, 2H), 2.72 (t, J = 7.5), 1.61 (m), 1.31 (m), 0.89 (m). HREIMS calcd, 667.9599; found, 667.9577 (M^+). Anal. Calcd for $C_{24}H_{30}I_2S_3$: C, 43.12; H, 4.52. Found: C, 43.79; H, 4.51.

3,3′,3″-Trihexyl-5,5″-diiodo-2,2′:5′,2″-terthiophene (2I). A solution of **2** (1.50 g, 2.99 mmol) and 50 mL of dichloromethane was cooled to 0 °C, and *N*-iodosuccinimide (1.48 g, 6.59 mmol) was added. Glacial acetic acid (1.12 mL, 19.8 mmol) was slowly added dropwise via syringe. The ice bath was removed, and the reaction mixture was allowed to stir at room temperature in the dark. The solvent was removed via rotary evaporation, and the resulting oil was redissolved in 30 mL of dichloromethane. After 1 h, the solution was washed with saturated aqueous Na_2CO_3 (2 × 50 mL) and dried with $MgSO_4$. The solvent was removed by rotary evaporation, and the resulting oil was purified by filtering through a short pad of silica with dichloromethane to provide 2.05 g (91%) of **2I** as a yellow-brown oil. ^{1}H NMR (300 MHz, $CDCl_3$): δ 7.12 (s, 1H), 7.07 (s, 1H), 6.90 (s, 1H), 2.71 (m), 2.50 (m), 1.55 (m), 1.26 (m), 0.88 (m). HREIMS $C_{30}H_{42}I_2S_3$ calcd, 752.0538; found, 752.0534 (M^+).

5,5″-Dibromo-3,3′,3″-trihexyl-2,2′:5′,2″-terthiophene (2Br). *N*-Bromosuccinimide was added in portions to **2** (300 mg, 0.60 mmol) in a solution of chloroform and acetic acid (15 mL, 1:1 v/v) at room temperature. After being stirred for 1 h, the reaction mixture was poured into water and extracted with hexane. The extracts were shaken with aqueous saturated Na_2CO_3, washed with brine, and dried with $MgSO_4$. The residue obtained after removal of the solvents was chromatographed on silica gel (3.8 × 25 cm) with hexane to afford 315 mg (80%) of the dibromo compound **2Br** as a pale yellow oil. ^{1}H NMR (300 MHz, $CDCl_3$): δ 6.93 (s, 1H, Th−H), 6.89 (s, 1H, Th−H), 6.88 (s, 1H, Th−H), 2.69 (t, 2H, J = 7.5, CH_2C$_5$H$_{11}$), 2.50−2.45 (m, 4H, CH_2C$_5$H$_{11}$), 1.61−1.26 (m, 24H, CH$_2$−(CH_2)$_4$−CH$_3$), 0.89−0.83 (m, 9H, CH$_3$). UV−vis (THF, nm (ϵ/(M^{-1} cm^{-1}))): 247 (7800), 318 (14 300). IR (neat, cm^{-1}): ν = 2955, 2925, and 2855 (C−H). EI-MS: *m*/*z*, 656 (M^+), 658 ($M + 2^+$), and 660 ($M + 4^+$) for $C_{30}H_{42}Br_2S_3$ based on ^{79}Br. Anal. Calcd for $C_{30}H_{42}Br_2S_3$: C, 54.71; H, 6.43. Found: C, 54.55; H, 6.60.

3,4′,4″-Trihexyl-5,5″-diiodo-2,2′:5′,2″-terthiophene (3I). A solution of **3** (500 mg, 0.998 mmol) in 30 mL of dichloromethane under Ar was cooled to 0 °C, and *N*-iodosuccinimide (494 mg, 2.20 mmol) was added. Glacial acetic acid (0.37 mL, 6.59 mmol) was slowly added dropwise via syringe. The ice bath was removed, and the reaction mixture was allowed to stir at room temperature in the dark. After 20 h, the solution was washed with saturated aqueous Na_2CO_3 (2 × 30 mL) and dried with $MgSO_4$. The solvent was removed by rotary evaporation, and the resulting oil was purified by filtering through a short pad of silica with hexanes followed by dichloromethane to yield 721 mg (96%) of **3I** as a yellow oil. ^{1}H NMR (300 MHz, $CDCl_3$): δ 7.07 (s, 1H), 6.86 (s, 1H), 6.77 (s, 1H), 2.71 (m), 2.55 (m), 1.61 (m), 1.32 (m), 0.90 (m). HREIMS calcd, 752.0538; found, 752.0597 (M^+). Anal. Calcd for $C_{30}H_{42}I_2S_3$: C, 47.87; H, 5.62. Found: C, 47.05; H, 5.54.

3,3‴-Dihexyl-5,5‴-diiodo-2,2′:5′,2″:5″,2‴-quaterthiophene (4I). A solution of **4** (1.00 g, 2.00 mmol) in 20 mL of dichloromethane was cooled to 0 °C, and *N*-iodosuccinimide (925 mg, 4.11 mmol) was added. Glacial acetic acid (0.75 mL, 13.3 mmol) was slowly added dropwise via syringe. The ice bath was removed, and the reaction mixture was allowed to stir at room temperature. After 4 h, the solvent was removed via rotary evaporation. The resulting solid was suspended in methanol and filtered, and then purified using column chromatography (silica gel/3:1 dichloromethane:hexanes) which yielded 873 mg (58%) of **4I** as a bright orange solid. ^{1}H NMR (300 MHz, $CDCl_3$): δ 7.11 (d, 2H,

(22) Barbarella, G.; Bongini, A.; Zambianchi, M. *Macromolecules* **1994**, *27*, 3039−3045.
(23) Azumi, R.; Götz, G.; Debaerdemaeker, T.; Bäuerle, P. *Chem.-Eur. J.* **2000**, *6*, 735−744.
(24) Kokubo, H.; Yamamoto, T. *Macromol. Chem. Phys.* **2001**, *202*, 1031−1034.

J = 3.9), 7.08 (s, 2H), 6.97 (d, 2H, J = 3.6), 2.73 (t, J = 7.8), 1.61 (m), 1.31 (m), 0.89 (t, J = 6.6). UV−vis (CH_2Cl_2, nm (ϵ/(M^{-1} cm^{-1})): 252 (18 000), 387 (37 000). HRFABMS calcd, 749.94764; found, 749.94692 (M^+). Anal. Calcd for $C_{28}H_{32}I_2S_4$: C, 44.80; H, 4.30; I, 33.81. Found: C, 45.12; H, 4.13; I, 34.07.

5,5″-Bis(dicyanomethylene)-3,3″-dihexyl-5,5″-dihydro-2,2′:5′,2″-terthiophene (Q1). To a suspension of sodium hydride (174 mg, 60% in oil, 4.34 mmol) in 1,2-dimethoxyethane (25 mL) was added malononitrile (119 mg, 1.80 mmol) at 0 °C under Ar. In a separate round-bottom flask, diiodo compound **1I** (500 mg, 0.748 mmol) was added to $Pd(PPh_3)_4$ (69 mg, 0.060 mmol) and 25 mL of 1,2-dimethoxyethane. The reaction mixture was degassed and heated to reflux. The sodium hydride solution was cannulated into the solution of **1I**, and the resulting solution was heated under reflux for 2 h. The resulting dark red mixture was cooled to 0 °C, and 25 mL of saturated Br_2/H_2O solution was added dropwise. The solution turned dark blue, and a precipitate formed. The suspension was filtered through a short pad of diatomaceous earth, washed with water (2 × 15 mL), and purified using column chromatography (silica gel/100% dichloromethane) to yield 268 mg (68%) of **Q1** as a metallic green solid. ^{1}H NMR (300 MHz, $C_2D_2Cl_4$, 100 °C): δ 7.46 (s, 2H), 7.18 (s, 2H), 2.87 (t, J = 7.8), 1.81 (quintet, J = 7.5), 1.45 (m), 0.99 (t, J = 6.9). UV−vis (CH_2Cl_2, nm (ϵ/(M^{-1} cm^{-1})): 546 sh, 594 sh, 648, 689 sh. HREIMS calcd, 542.1633; found, 542.1631 (M^+). Anal. Calcd for $C_{30}H_{30}N_4S_3$: C, 66.38; H, 5.57; N, 10.32. Found: C, 66.42; H, 5.43; N, 10.07.

5,5″-Bis(dicyanomethylene)-3,3′,3″-trihexyl-5,5″-dihydro-2,2′:5′,2″-terthiophene (Q2). Compound **Q2** was prepared by two different methods.

Method A.[18,25,26] To a suspension of sodium hydride (89 mg, 60% in oil, 2.2 mmol) in 1,2-dimethoxyethane (15 mL) was added malononitrile (66 mg, 1.0 mmol) at 0 °C. The mixture was allowed to warm to room temperature, and **2Br** (264 mg, 0.40 mmol) and $Pd(PPh_3)_4$ were added successively. The reaction was heated at reflux for 4 h. The resulting mixture was extracted with chloroform, washed with brine, and dried with $MgSO_4$. The dark solid obtained after removal of the solvents was chromatographed on silica gel (3.8 × 22 cm) with hexane/chloroform (5:3) to afford 62 mg (26%) of the quinoid compound **Q2**, which was recrystallized from hexane/chloroform as a dark microcrystalline powder.

Method B. To a suspension of sodium hydride (464 mg, 60% in oil, 11.6 mmol) in 1,2-dimethoxyethane (60 mL) was added malononitrile (316 mg, 4.78 mmol) at 0 °C under Ar. In a separate round-bottom flask, diiodo compound **2I** (1.50 g, 1.99 mmol) was added to $Pd(PPh_3)_4$ (184 mg, 0.159 mmol) and 50 mL of 1,2-dimethoxyethane and heated to reflux under Ar. The sodium hydride solution was cannulated into the solution of **2I**, and the resulting solution was heated under reflux for an additional 2 h. The resulting dark red mixture was cooled to 0 °C, and 50 mL of saturated Br_2/H_2O solution was added dropwise. The solution turned dark blue, and a precipitate formed. The suspension was filtered through a frit, and the isolated solid was washed with water (4 × 15 mL) to yield 1.51 g of crude solid. A 200 mg portion of the crude solid was filtered through a short pad of silica with dichloromethane, and then further purified using column chromatography (silica gel/100% dichloromethane) to yield 82 mg (50%) of **Q2** as a dark solid. ^{1}H NMR (300 MHz, $C_2D_2Cl_4$, 100 °C): δ 7.29 (s, 1H), 7.21 (s, 1H), 7.15 (s, 1H), 2.99 (t, J = 7.5), 2.86 (t, J = 7.8), 1.81 (m), 1.49 (m), 0.99 (m). UV−vis (CH_2Cl_2, nm): 669. UV−vis (THF, nm (ϵ/(M^{-1} cm^{-1})): 600 sh (42 700), 660 (94 300). EIMS 627 (M^+), 628 ($M + 1^+$), 629 ($M + 2^+$). IR (KBr, cm^{-1}) ν = 2210 (C≡N). Anal. Calcd for $C_{36}H_{42}N_4S_3$: C, 68.97; H, 6.75; N, 8.94. Found: C, 68.71; H, 6.70; N, 8.72.

5,5″-Bis(dicyanomethylene)-3,4′,4″-trihexyl-5,5″-dihydro-2,2′:5′,2″-terthiophene (Q3). To a suspension of sodium hydride (183 mg, 60% in oil, 4.60 mmol) in 1,2-dimethoxyethane (20 mL) was added malononitrile (126 mg, 1.90 mmol) at 0 °C under Ar. The reaction mixture was removed from the ice bath and stirred for 10 min, and then **3I** (600 mg, 0.79 mmol) and $Pd(PPh_3)_4$ (73 mg, 0.063 mmol) were added. The mixture was heated under reflux for 3.5 h. The resulting dark red mixture was cooled to 0 °C, and 30 mL of saturated Br_2/H_2O solution was added dropwise. The solution turned blue, and a precipitate formed. The suspension was filtered through a short pad of diatomaceous earth, washed with water (1 × 30 mL), and purified using column chromatography (silica gel/100% dichloromethane) to yield 262 mg (53%) of **Q3** as a metallic green solid. ^{1}H NMR (300 MHz, $C_2D_2Cl_4$, 100 °C): δ 7.34 (s, 1H), 7.22 (s, 1H), 7.13 (s, 1H), 2.96 (t, J = 7.5), 2.85 (m), 1.78 (m), 1.49 (m), 0.99 (m). UV−vis (CH_2Cl_2, nm (ϵ/(M^{-1} cm^{-1})): 537 sh, 581 sh, 640 sh, 672 (93 000), 768 sh. HREIMS calcd, 626.2572; found, 626.2596 (M^+). Anal. Calcd for $C_{36}H_{42}N_4S_3$: C, 68.97; H, 6.75; N, 8.94. Found: C, 68.44; H, 6.56; N, 8.70.

5,5‴-Bis(dicyanomethylene)-3,3‴-dihexyl-5,5‴-dihydro-2,2′:5′,2″:5″,2‴-quaterthiophene (Q4). To a suspension of sodium hydride (93 mg, 60% in oil, 2.32 mmol) in 1,2-dimethoxyethane (15 mL) was added malononitrile (64 mg, 0.96 mmol) at 0 °C under Ar. The reaction mixture was removed from the ice bath, was stirred for 0.5 h, and then **4I** (300 mg, 0.40 mmol) and $Pd(PPh_3)_4$ (370 mg, 0.32 mmol) were added. The mixture was heated under reflux for 3.5 h. The resulting dark red mixture was cooled to 0 °C (via ice bath), and 20 mL of saturated Br_2/H_2O solution was added dropwise. The solution turned blue, and a precipitate formed. An additional 40 mL of water was added to the suspension while stirring. The suspension was filtered and washed with water (3 × 10 mL). The dark blue solid was purified using column chromatography by sequentially eluting the column with 100% CH_2Cl_2, 5/95 ethyl acetate/CH_2Cl_2, and 10/90 ethyl acetate/CH_2Cl_2 to yield 68 mg (30%) of **Q4** as a dark solid. UV−vis (CH_2Cl_2, nm (ϵ/(M^{-1} cm^{-1})): 709 sh, 779 (190 000), 867 sh. HRFABMS calcd ($[C_{34}H_{32}N_4S_4+H]^+$), 625.1588; found, 625.1594. LRFABMS calcd ($[C_{34}H_{31}BrN_4S_4+H]^+$), 704.8; found, 705.1; calcd ($[C_{34}H_{30}Br_2N_4S_4+H]^+$), 783.7; found, 784.0. Anal. Calcd for $C_{34}H_{31.76}Br_{0.24}N_4S_4$: C, 63.44; H, 4.97; N, 8.71. Found: C, 63.53; H, 5.05; N, 8.24.

X-ray Structure Determinations. Relevant crystallographic data are shown in Table 1. All crystals were grown by slow evaporation of saturated solutions (**Q1**, CH_3CN/CH_2Cl_2; **Q2**, CH_2Cl_2; **Q3**, CH_2Cl_2/*n*-heptane; **Q3tol**, CH_2Cl_2/toluene; **Q4**, CH_2Cl_2). The data for the single-crystal X-ray structures of **Q2**, **Q3**, and **Q4** were collected at the APS synchrotron sector 15-ID-C at Argonne National Laboratory due to the extremely small size of at least one crystal dimension. In each case, the crystals used for the synchrotron structure determinations were obtained after months of attempts with different solvents and methods of crystallization. Single crystals were attached to glass fibers and mounted on the Bruker Kappa/SMART 6000 microdiffractometer for data collection at 100 K using double diamond-monochromated Ag Kα radiation (λ = 0.5500 Å). An initial set of cell constants was calculated from reflections harvested from three sets of 65 frames oriented such that orthogonal wedges of reciprocal space were surveyed. Final cell constants were calculated from a minimum of 2033 strong reflections from the actual data collection. Data were collected to the extent of 2.0 hemispheres at a resolution of 0.80 Å using ϕ-scans.

Somewhat larger crystals were available for **Q1** and **Q3tol**; the data for these structure determinations were collected at the X-ray Crystallographic Laboratory (Department of Chemistry, University of Minnesota). Single crystals were attached to glass fibers and mounted on the Siemens SMART system for data collection at 173 K using graphite-monochromated Mo Kα radiation (λ = 0.71073 Å). An initial set of cell constants was calculated from reflections harvested from three sets of 20 frames oriented such that orthogonal wedges of reciprocal space were surveyed. Final cell constants were calculated from a minimum set of 765 strong reflections from the actual data collection. Data were collected to the extent of 1.5−2.0 hemispheres at a resolution of 0.84 Å using ϕ-scans.

(25) Higuchi, H.; Yoshida, S.; Uraki, Y.; Ojima, J. *Bull. Chem. Soc. Jpn.* **1998**, *71*, 2229−2237.
(26) Yui, K.; Aso, Y.; Otsubo, T.; Ogura, F. *Bull. Chem. Soc. Jpn.* **1989**, *62*, 1539−1546.

Table 1. X-ray Data Collection and Refinement

compound	Q1	Q2	Q3	Q3tol	Q4
formula	$C_{30}H_{30}N_4S_3$	$C_{36}H_{42}N_4S_3$	$C_{36}H_{42}N_4S_3$	$C_{36}H_{42}N_4S_3 \cdot C_7H_8$	$C_{34}H_{30.8}Br_{0.24}S_4$
habit	plate	ribbon	plate	rod	needle
color	metallic green	aqua	metallic green	metallic green	metallic
lattice type	triclinic	triclinic	triclinic	triclinic	monoclinic
space group	$P\bar{1}$	$P\bar{1}$	$P\bar{1}$	$P\bar{1}$	$P2_1/c$
a, Å	7.951(3)	6.555(2)	5.6513(9)	8.4670(14)	6.2902(10)
b, Å	13.212(4)	14.858(7)	15.832(3)	12.873(2)	8.6138(11)
c, Å	13.936(4)	18.269(8)	19.096(3)	19.364(5)	29.089(4)
α, deg	95.876(6)	93.214(16)	98.562(7)	104.072(15)	90
β, deg	98.489(6)	96.441(17)	90.409(7)	102.560(14)	94.301(6)
γ, deg	97.492(6)	94.512(17)	93.139(7)	96.391(14)	90
V, Å^3	1424.6(8)	1758.8(13)	1686.7(5)	1967.9(7)	1571.7(4)
Z	2	2	2	2	2
formula wt, g mol^{-1}	542.76	626.92	626.92	719.05	642.84
D_c, g cm^{-3}	1.265	1.184	1.234	1.213	1.358
temp (K)	173(2)	100(2)	100 (1)	173(2)	100(2)
μ, mm^{-1}	0.286	0.130	0.135	0.224	0.340
F (000)	572	668	668	768	670
θ range, deg	1.49−25.07	0.88−19.58	2.56−20.18	1.12−25.05	1.09−21.25
index ranges	$-9 \le h \le 9$	$-7 \le h \le 7$	$-7 \le h \le 7$	$-10 \le h \le 9$	$-7 \le h \le 8$
	$-15 \le k \le 15$	$-17 \le k \le 17$	$-19 \le k \le 19$	$-15 \le k \le 12$	$-11 \le k \le 11$
	$-16 \le l \le 16$	$0 \le l \le 21$	$0 \le l \le 23$	$-23 \le l \le 22$	$-37 \le l \le 38$
reflns collected	14 280	30 111	22 100	11 945	18 073
unique reflns	5062	5743	6804	6872	3588
	($R_{int} = 0.0745$)	($R_{int} = 0.0597$)	($R_{int} = 0.0444$)	($R_{int} = 0.0277$)	($R_{int} = 0.0729$)
weighting factors,[a] a,b	0.0488, 0.000	0.0886, 6.2076	0.0825, 1.2263	0.0483, 0.9547	0.0772, 3.2773
max, min transmission	1.0000, 0.8903	0.9987, 0.9923	0.9997, 0.9866	1.0000, 0.8602	0.9966, 0.9668
data/restraints/parameters	5062/9/353	5743/63/407	6804/0/391	6872/1/451	3588/0/215
R_1, wR_2 ($I > 2\sigma(I)$)	0.0503, 0.0947	0.0789, 0.2150	0.0466, 0.1295	0.0560, 0.1175	0.0725, 0.1943
R_1, wR_2 (all data)	0.1434, 0.1215	0.1082, 0.2388	0.0606, 0.1387	0.0880, 0.1270	0.0939, 0.2092
GOF	0.963	1.104	1.000	1.043	1.210
largest diff peak, hole, e Å^{-3}	0.204, −0.367	1.135, −0.736	0.634, −0.423	0.413, −0.296	0.620, −0.459

[a] $w = [\sigma^2(F_o^2) + (aP)^2 + (bP)]^{-1}$, where $P = (F_o^2 + 2F_c^2)/3$.

For all structures, the intensity data were corrected for absorption and decay using SADABS.[27] Space groups were determined on the basis of systematic absences and intensity statistics. Direct-methods solutions provided the positions of most non-hydrogen atoms. Several full-matrix least-squares/difference Fourier cycles were performed to locate the remaining non-hydrogen atoms. All calculations were performed using the SHELXTL-V5.0 suite of programs[28] on Pentium computers. ORTEP diagrams that show the atomic numbering schemes are shown in the Supporting Information.

Packing analysis parameters were measured using SHELXTL, Mercury,[29] Cerius^2 v3.0,[30] and Excel. All π-stacking distances were measured in the following way: least-squares planes were calculated from the atoms in the backbone of the quinoidal molecules (terthiophenes using S1−3, N1−4, C1−18; quaterthiophene, S1−2, S1A−2A, N1−2, C1−11, C1A−11A). The perpendicular distance between adjacent planes was then calculated from the equations of the planes. In all of the structures, the least-squares planes of the quinoidal backbone are exactly parallel. The method of analyzing the distortions of these structures from an ideal cofacial π-stack was adapted from Curtis et al.[15] The pitch and roll distances measure the translations along the long and short molecular axes, respectively, from an ideal cofacial stack. Pitch and roll distances were calculated from orthogonal atom coordinates (SHELX) with the origin set at the geometric centroid of the backbone atom positions.

Additionally, a simple model to approximate the area overlap of adjacent π-stacking molecules is introduced. Each molecule is treated as a rectangle with the long molecular axis treated as the long axis of the rectangle. The parallel spatial overlap of molecules in adjacent planes is approximated by the area overlap of the molecular rectangles. The calculated parallel area overlaps range from 0 to 1, where 1 is interpreted as complete overlap of the molecules in adjacent planes (pitch distance = 0, roll distance = 0). The calculated area overlaps are relative to the specific molecule, so three and four ring systems can be compared. For terthiophenes, the length of the rectangle was defined as the distance between atoms C3 and C16, and the width was calculated as the distance between the C6/C13 centroid and the C9/C10 centroid. For the quaterthiophene, the length of the rectangle was defined as the distance between atoms C3 and C3A, and the width was calculated as the sum of the distances from the inversion center (at the center of the molecule), perpendicular to the long molecular axis, to atoms C6 and C10.

A "molecular volume" overlap was also calculated from the product of the area overlap and a distance derived from the π-stacking axis. The overlap in the stacking direction was calculated by subtracting the π-stacking distance from 4 Å, an arbitrary distance at which the interaction between adjacent layers was considered zero. An accepted measure of the packing efficiency[31] was also calculated and analyzed for X-ray structural comparisons. The Kitaigorodskii packing coefficient is defined by the following equation: $C_K = (Z^*V_c)/V$, where C_K is the Kitaigorodskii packing coefficient, Z is the number of formula units in the unit cell, V_c is the volume occupied by the atoms in the unit cell, and V is the volume of the unit cell. The volume occupied by a molecule was calculated within a van der Waals surface for each molecule using Cerius^2 software.

Computational Details

As detailed in previous works, we use the semiempirical Hartree−Fock INDO method (as developed by Zerner and co-workers for spectroscopic purposes[32]) to compute the electronic structure of isolated molecules and of supermolecular systems made of dimers or larger molecular clusters. The atomic coordinates of isolated molecules and

(27) (a) Sheldrick, G. *SADABS v.2.03*; 2002. (b) Blessing, R. *Acta Crystallogr.* **1995**, *A51*, 33−38.
(28) *SHELXL v.6.1*; Bruker AXS, Madison, WI, 2001.
(29) New software for searching the Cambridge Structural Database and visualizing crystal structures. Bruno, I. J.; Cole, J. C.; Edgington, P. R.; Kessler, M. K.; Macrae, C. F.; McCabe, P.; Pearson, J.; Taylor, R. *Acta Crystallogr.* **2002**, *B58*, 389−397.
(30) *Cerius^2 v3.0 software*; Molecular Simulations Inc., San Diego, CA.
(31) Kitaigorodskii, A. I. *Organic Chemical Crystallography*; Consultants Bureau Enterprises: New York, 1961.
(32) (a) Ridley, J.; Zerner, M. C. *Theor. Chim. Acta* **1973**, *32*, 111−134. (b) Zerner, M. C.; Loew, G. H.; Kichner, R. F.; Mueller-Westerhoff, U. T. *J. Am. Chem. Soc.* **1980**, *102*, 589−599.

Table 2. Electrochemistry and UV−Vis Data for Quinoidal Oligothiophenes

			oxidation processes (volts)		reduction processes (volts)	
compound	rings	alkyl chains	$E_1°$	$E_2°$	$E_1°$ ($E_2°$)	λ_{max} (nm)[a]
DCMT[b]	3	2	1.27	1.96[c]	−0.15[d]	670
Q1[b]	3	2	1.32	1.92[c]	−0.20[d]	648
Q2[b]	3	3	1.27	1.86[c]	−0.18[d]	669
Q3[b]	3	3	1.23	1.81[c]	−0.23[d]	672
Q4[b]	4	2	0.99	1.55	0.06 (−0.09)	779
DCMQ[e]	4	4	f	f	−0.07 (−0.18)	790[g]
DCMQ[h]	4	4	0.83	1.37	−0.086[d]	790

[a] Values from solution in CH_2Cl_2, unless otherwise indicated. [b] Scan rate of 100 mV/s (ambient temp) in $TBAPF_6$ at a glassy carbon working electrode. [c] Irreversible, E_{pa} value is given. [d] Two-electron process. [e] Scan rate of 100 mV/s (ambient temp) in $TBAClO_4$ at a platinum working electrode, ref 18. [f] Value not reported. [g] Value in THF solution. [h] Scan rate of 10 mV/s (ambient temp) in $TBAPF_6$ at a glassy carbon working electrode, ref 17.

larger clusters were all taken from the experimental X-ray structures. No geometry optimizations were performed.

The choice of the INDO/S Hamiltonian is driven by the fact that INDO calculations have been shown to provide descriptions of the one-electron structure of isolated and interacting conjugated molecules in excellent agreement with corresponding experimental data[14,33] and theoretical data obtained at the ab initio level.[34]

Results and Discussion

Oligomer Synthesis. The precursors to the quinoid products were prepared by iodination (compounds **1I**−**4I**) or bromination (**2Br**) of their respective parent oligothiophenes (compounds **1**−**4**) with *N*-iodosuccinimide or *N*-bromosuccinimide in a 1:1 acetic acid/dichloromethane solution.[18,25,26] Filtration through silica gel removed succinimide and gave the halogenated oligomers in good yields (57−96%). Of special interest is the synthesis of the HT-regioregular oligomer **3**. The syntheses of the regioregular precursors (**A**−**G**) followed a general scheme previously reported for *n*-octyl oligothiophene analogues.[20]

The title compounds **Q1**−**Q4** (Figure 1) were prepared by procedures previously developed for similar molecules.[18,25,26] Palladium-catalyzed cross-coupling of sodium malonate to the precursors affords a thienyl malononitrile that is deprotonated in-situ by sodium hydride. The success of the reaction is indicated by the formation of a dark orange fluorescent solution of the doubly reduced quinoid dianion intermediate. Oxidation of the dianion with excess bromine/water afforded the neutral quinoid forms **Q1**−**Q4**. In the case of quaterthiophene **Q4**, partial electrophilic substitution of the 4 and 4‴ sites occurred to give approximately 11.9% bromination, according to both the X-ray and the elemental analysis data. The presence of monobromo- and dibromo-substituted species was observed in the mass spectrum of **Q4**. No evidence for bromination of **Q1**, **Q2**, or **Q3** was observed.

Electrochemical Properties. Cyclic voltammograms (CVs) of oligomers **Q1**, **Q2**, **Q3**, and **Q4** were measured in 0.1 M $TBAPF_6$ solutions in CH_2Cl_2. The electrochemical data of these compounds as well as the related compounds 3′,4′-dibutyl-5,5″-bis(dicyanomethylene)-5,5″-dihydro-2,2′:5,2″-terthiophene (**DCMT**) and **DCMQ** are summarized in Table 2. The CVs of **Q1**, **Q2**, and **Q3** (Figure 2) each exhibit a reversible one-electron oxidation process near 1.3 V, a second less-reversible oxidation

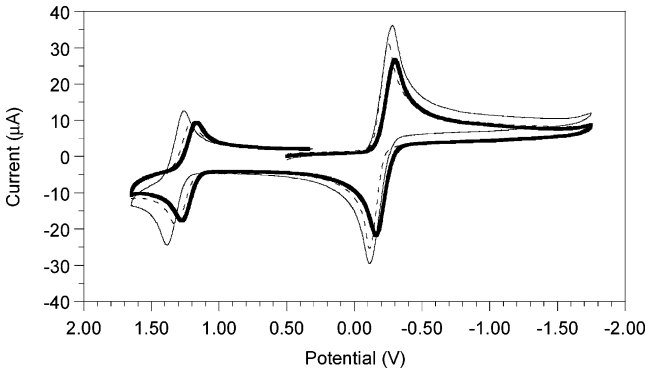

Figure 2. Cyclic voltammograms of **Q1** (solid line), **Q2** (dashed line), and **Q3** (solid bold line). Scans are initiated from +0.50 V in the negative direction.

near 1.9 V (not shown), and a reversible two-electron reduction process near −0.2 V. The relative number of electrons transferred in these processes was confirmed by Osteryoung square wave voltammetry. The first oxidative process generates a stable cation radical by oxidation of the π-system, while the second oxidative process generates a less stable dication. The two-electron reduction process involves reduction of the π-system to a dianion that is stabilized by the electron-withdrawing dicyanomethylene groups. Slower or faster scan rates did not resolve the two-electron process into separate one-electron reductions. This suggests that the formal potentials for the first and second reduction processes are inverted so that the one-electron reduced species undergoes a facile disproportionation reaction at the electrode surface.

The number and position of hexyl substituents subtly tune the electrochemical properties of these molecules. In general, the first oxidation is easier for molecules with three versus two hexyl groups. If it is assumed that the electron-donating ability of a butyl group is similar to a hexyl group, then the effect of substitution on the oxidation potential can be attributed to both the number and the position of alkyl chains. A comparison of **DCMT** with **Q1**, both with two alkyl groups, indicates that the location of the alkyl group influences the oxidation. The center-ring ortho-dialkyl-substituted **DCMT** oxidizes at slightly lower potential (1.27 vs 1.32 V for **Q1**). Alkylation of the center ring of **Q1** to give **Q2** lowers the oxidation potential, making it equal to **DCMT**. Monoalkylation of all rings in a head-to-tail fashion (**Q3**) has the greatest effect and gives the lowest oxidation potential of all of the terthiophene quinoids studied here. Changes in the potential of the reduction process are also small and not merely the reverse of the oxidation trend. In general, the position of the alkyl substituent has a rather small effect; increasing the number of rings from three to four produces a much larger effect and reinforces the idea that the quinoidal oligothiophenes are neutral-stabilized oligothiophene dications.

Extension of the π-system to a longer oligothiophene quinoid system also greatly decreases the redox potentials, particularly the oxidations. **Q4** exhibits two sequential reversible one-electron oxidation processes at $E°′ = 0.99$ and 1.55 V and two very closely spaced sequential reversible reduction processes at $E°′ = 0.06$ and −0.09 V. The relative number of electrons transferred in the processes of **Q4** was confirmed by Osteryoung square wave voltammetry. The electrochemical behavior of **Q4** is also quite similar to the related molecule **DCMQ**[17,18] that displays a two-electron reduction under experimental conditions

(33) Cornil, J.; Calbert, J. P.; Brédas, J. L. *J. Am. Chem. Soc.* **2001**, *123*, 1250−1251.
(34) Newton, M. D. *Int. J. Quantum Chem.* **2000**, *77*, 255−263.

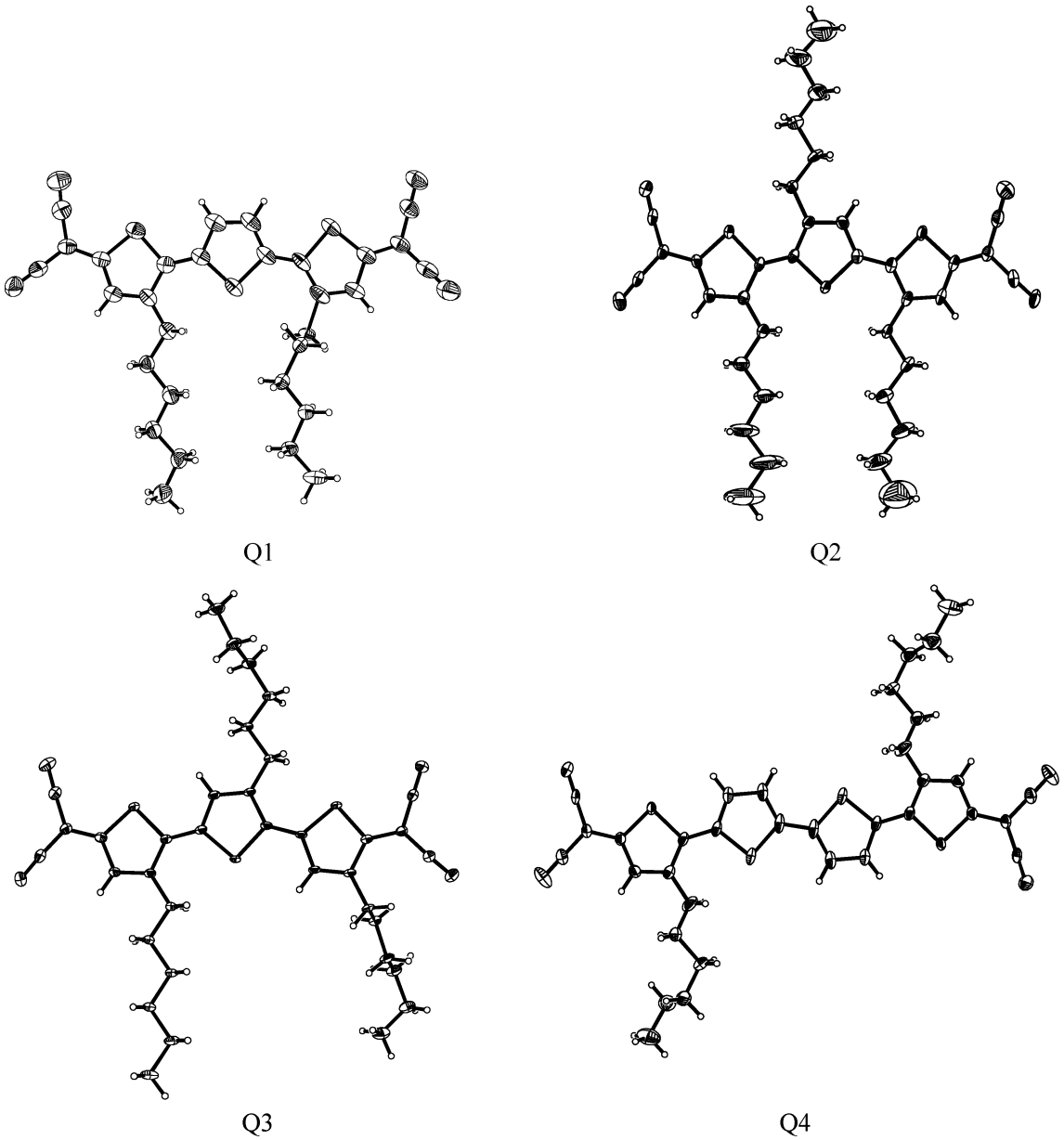

Figure 3. ORTEP diagrams of **Q1**, **Q2**, **Q3**, and **Q4** (50% ellipsoids). Ellipsoids appear small for **Q2**, **Q3**, and **Q4** as the structure data were acquired at 100 K. **Q1** structure data were acquired at 173 K.

nearly identical[17] to those used for **Q1**−**Q4**. The sensitivity of these sequential reduction processes to supporting electrolyte is also illustrated by **DCMQ**, which displays two separate one-electron reductions at a platinum working electrode with $TBAClO_4$ as the supporting electrolyte. Finally, the two additional electron-donating alkyl groups of **DCMQ** shift the oxidations to less positive potentials and the reductions to more positive potentials relative to **Q4**, resulting in a smaller electrochemical band-gap for **DCMQ**. In summary, changing the number of rings, and the position and number of the alkyl group substituents, is an effective way to tune the redox properties of these quinoidal oligothiophenes.

Electronic Spectra. Solution electronic spectral data for the oligomers in this study were measured and are collected in Table 2. All of the oligomers have similar solution electronic spectra that are dominated by an intense absorption ($\epsilon \cong 100\,000\ M^{-1}\ cm^{-1}$) attributed to a $\pi-\pi^*$ transition of the highly conjugated quinoidal π-system. The compound **Q1** with only two hexyl groups has a peak ($\lambda_{max} = 648$ nm) that is at slightly higher energy than the three hexyl group analogues **Q2** and **Q3** ($\lambda_{max} = 669$ and 672 nm, respectively). In agreement with the observed electrochemical measurements, the UV−vis spectrum of the parent compound **DCMT** with two butyl groups on the middle ring ($\lambda_{max} = 670$ nm)[16] is more like the three hexyl group-substituted molecules **Q2** and **Q3** than the end-ring-substituted **Q1**. In **Q4**, the extension of the π-system by an additional thiophene ring substantially lowers the energy of the $\pi-\pi^*$ transition ($\lambda_{max} = 779$ nm). The related **DCMQ**[17,18] ($\lambda_{max} = 790$ nm) electronic spectrum is very similar to that observed for **Q4**, but slightly shifted to lower energy as is the electrochemical band-gap.

X-ray Structural Details. A brief summary of each individual structure will be given followed by an analysis of the packing and intermolecular forces that are common to all. ORTEP diagrams are shown in Figure 3.

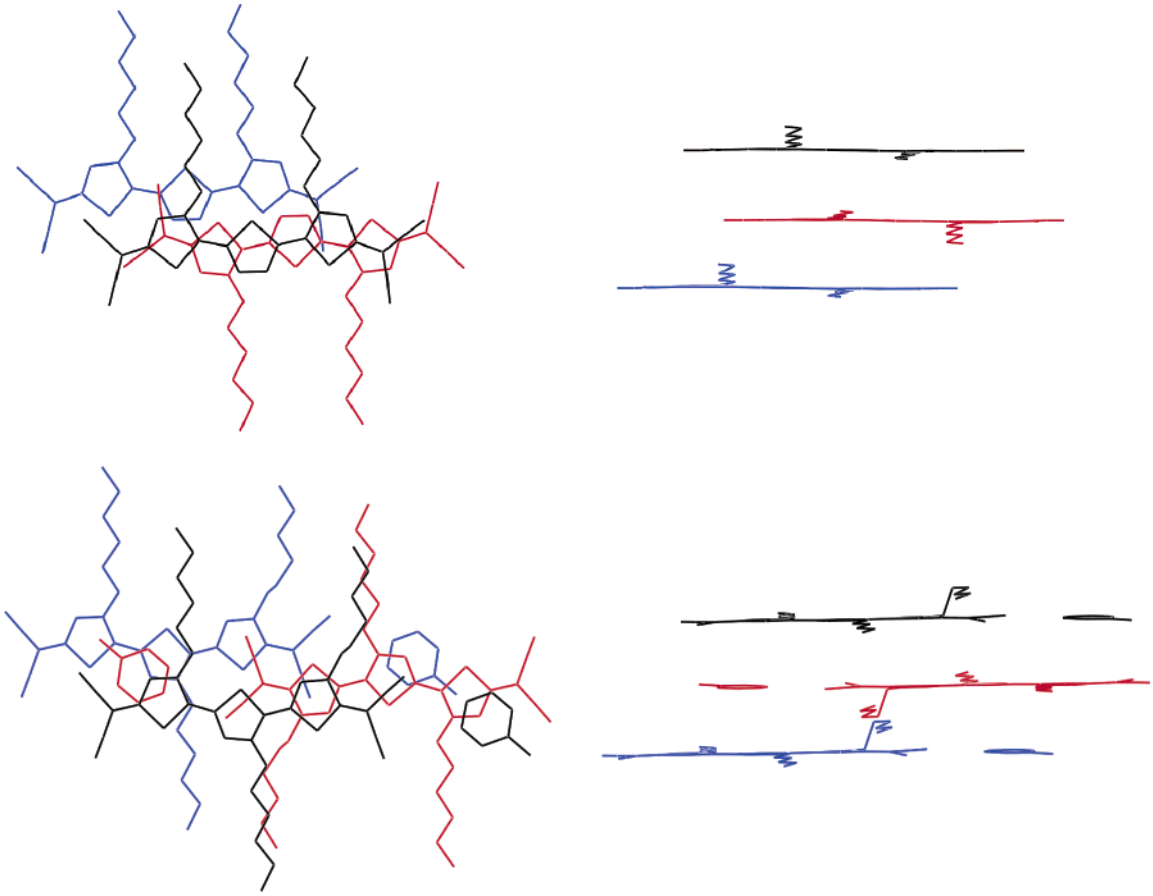

Figure 4. Stacking diagrams showing overlap in the direction parallel (left) and perpendicular (right) to the π-stacking for dimer structures **Q1** (upper) and **Q3tol** (lower).

The structure of **Q1** displays a very planar bis-dicyanomethyleneterthiophene backbone with a mean deviation from planarity of 0.0241 Å across all 25 atoms. Both of the inter-ring double bond linkages adopt the transoid geometry. Disorder for one of the hexyl chains was modeled over two positions with a 50.2/49.8 ratio. The disordered hexyl group adopts one conformation (C25′−C30′) that is virtually the same as the ordered hexyl group (C19−C24), while the other disorder conformation (C25−C30) has a kink in the hexyl group. The molecules pack (Figure 4) as π-dimers in a layered π-stacking arrangement with two alternating distances of 3.335 and 3.455 Å.

The backbone of **Q2** is quite planar with an average deviation from a least-squares plane of 0.0494 Å. Both of the inter-ring double bond linkages adopt the transoid geometry. The hexyl group substituent on the center ring is disordered over two sites with an occupancy ratio of 53.7/46.3. The disordered hexyl group adopts two very similar conformations (C25−C30, C25′−C30′) that are both essentially in the molecular plane of the quinoidal terthiophene backbone and the end-ring hexyl groups (C31−C36, C19−C24). In this case, the molecules pack (Figure 5) in layers with one unique π-stacking distance of 3.393 Å.

The structure of **Q3** shows the backbone is rather flat, with an average deviation from a least-squares plane of 0.0565 Å. Both of the inter-ring double bond linkages adopt the transoid geometry. One end-ring hexyl (C19−C24) is flat and lies in the plane of the backbone. The center-ring hexyl (C25−C30) and the other end-ring hexyl (C31−C36) are both kinked substantially out of the molecular plane. **Q3** packs (Figures 5, 6) in layers with one unique π-stacking distance of 3.492 Å.

When **Q3** is crystallized from toluene solutions, the toluene solvate structure (**Q3tol**) results. The structure of **Q3tol** contains one molecule of toluene in addition to one **Q3** molecule in the asymmetric unit. This terthiophene backbone is the most planar of all of the terthiophene structures reported here with a mean deviation from a least-squares plane of 0.0235 Å. Both of the inter-ring double bond linkages adopt the transoid geometry. Two hexyl groups are located in the plane of the backbone, while one (C31−C36) is kinked out of the plane. The toluene molecule π-stacks nicely with **Q3**, forming a layered structure similar to the unsolvated structure. The toluene molecule is almost coplanar with the **Q3** backbone (1.4° between least-squares planes formed by **Q3** and toluene); however, **Q3tol** displays two unique **Q3**−**Q3** distances (3.404, 3.465 Å) as well as two unique **Q3**−toluene distances (Figure 4).

An inversion center lies at the middle of the bond connecting the second and third thiophene rings of **Q4**; thus the asymmetric unit is one-half of one molecule and all three inter-ring double bond linkages adopt the transoid geometry. **Q4** is very flat with a mean deviation from a least-squares plane containing 30 atoms (all non-hydrogen atoms except bromine and the hexyl groups) of 0.0404 Å. The hexyl groups are disordered over two similar positions with an occupancy ratio of 51.8/48.2. The bulk sample from which these crystals were grown contains bromine (elemental analysis, mass spectroscopy), and electron density maps suggested that a partially occupied, symmetry related bromine atom is present in the 4 and 4‴ positions of the outer thiophene rings. The bromine atom was allowed to refine as a free variable, and the refined occupancy of 11.9% agrees well

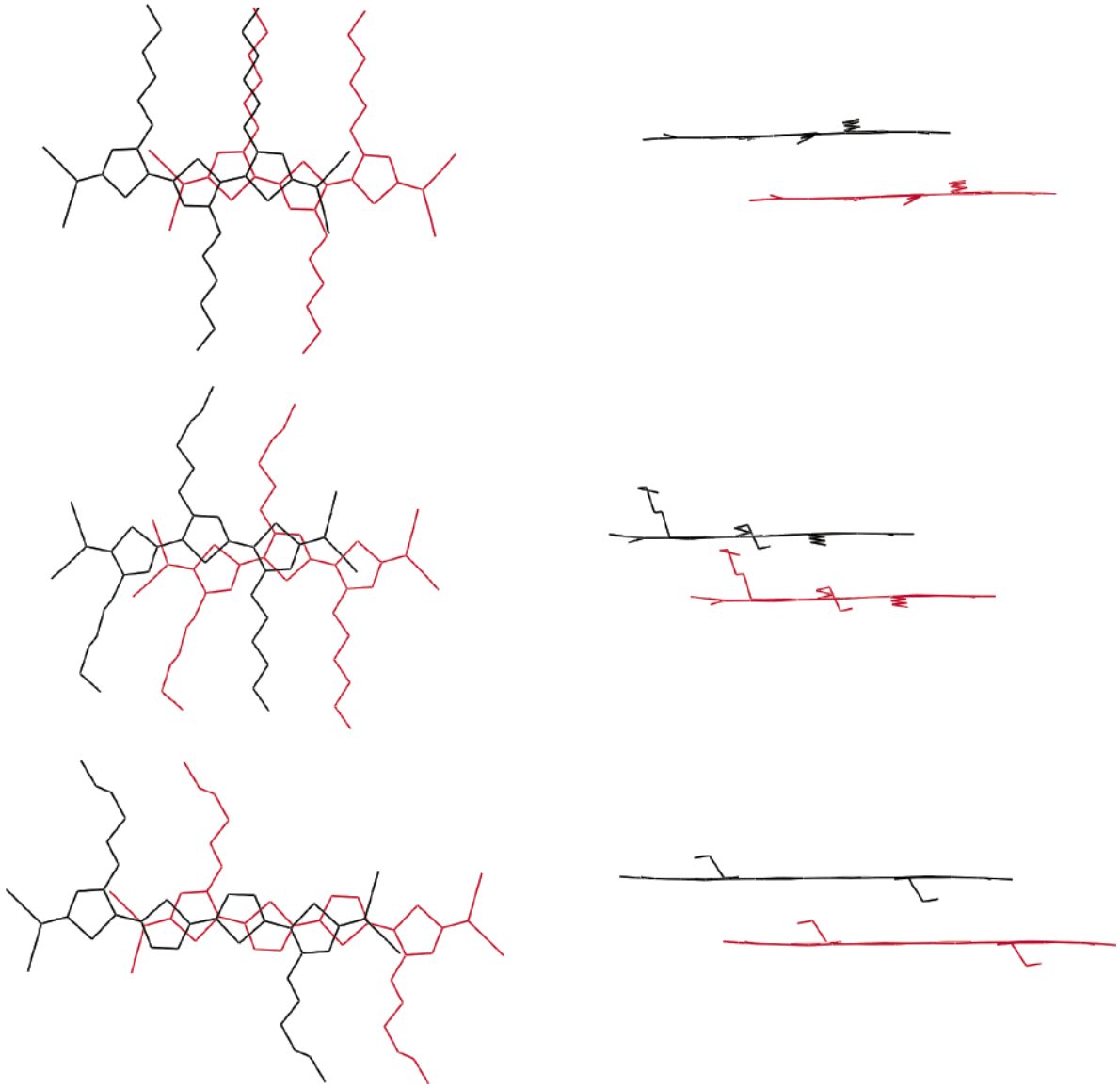

Figure 5. Stacking diagrams showing overlap in the direction parallel (left) and perpendicular (right) to the π-stacking for single-distance structures **Q2** (upper), **Q3** (middle), and **Q4** (lower).

with the combustion analysis. The remaining 88.1% occupancy was refined as a hydrogen atom in an ideal position for bonding with a thiophene carbon. **Q4** packs (Figure 6) in a herringbone structure with one unique π-stacking distance of 3.358 Å.

Structural Comparisons. Perhaps the simplest way to compare crystalline solids is to measure the packing efficiency.[31] The Kitaigorodskii packing coefficient (C_K) is calculated by dividing the occupied molecular volume (calculated from a van der Waals surface) by the total volume of the unit cell (calculated from the unit cell parameters). The packing coefficient does not distinguish between the types of interactions present but is a general measure of the quality of all of the intermolecular interactions present in a crystal lattice. The packing coefficients of **Q1**−**Q4** and other molecules of interest are compared in Table 3. All molecules in the table pack with relatively good efficiency. Aromatic molecules typically pack with coefficients in the range of 0.6−0.8.[31] The tightly packed structure of graphite has a packing coefficient of 0.887.[31] Although the three single π-distance quinoid structures show a correlation between the π-stacking distance and packing coefficient, the inclusion of BDT (3.530 Å, $C_K = 0.765$) and C5PTCDI (3.405 Å, $C_K = 0.704$)[35] indicates that this simple correlation only holds for molecules with very similar intermolecular interactions. An anisotropic analysis of the intermolecular features divides the forces into those along the stacking axis ($\pi-\pi$ interactions) and roughly perpendicular to the stacking axis (nonclassical hydrogen-bonding interactions). Our discussion of these structures will include the only other reported quinoidal oligothiophene structure with three or more thiophene rings, **DCMT**.[10,16]

The **Q1**−**Q4** structures reported here for the first time exhibit packing arrangements with extensive π-stacking (Figures 4−6). Structures **Q1**, **Q2**, **Q3**, and **Q3tol** all pack in π-stacked layers, but **Q4** (Figure 6) and **DCMT** pack as π-stacks arranged in the γ motif, a layered herringbone structure, vide infra. At this point, it is important to make the distinction between the herringbone structure of pentacene and that of **DCMT** and **Q4**. Desiraju

(35) Kitaigorodskii packing coefficients calculated using the Cerius[2] software and the CIF files for BDT (CCDC data code NOBJET) and C5PTCDI (CCDC data code DICMUX).

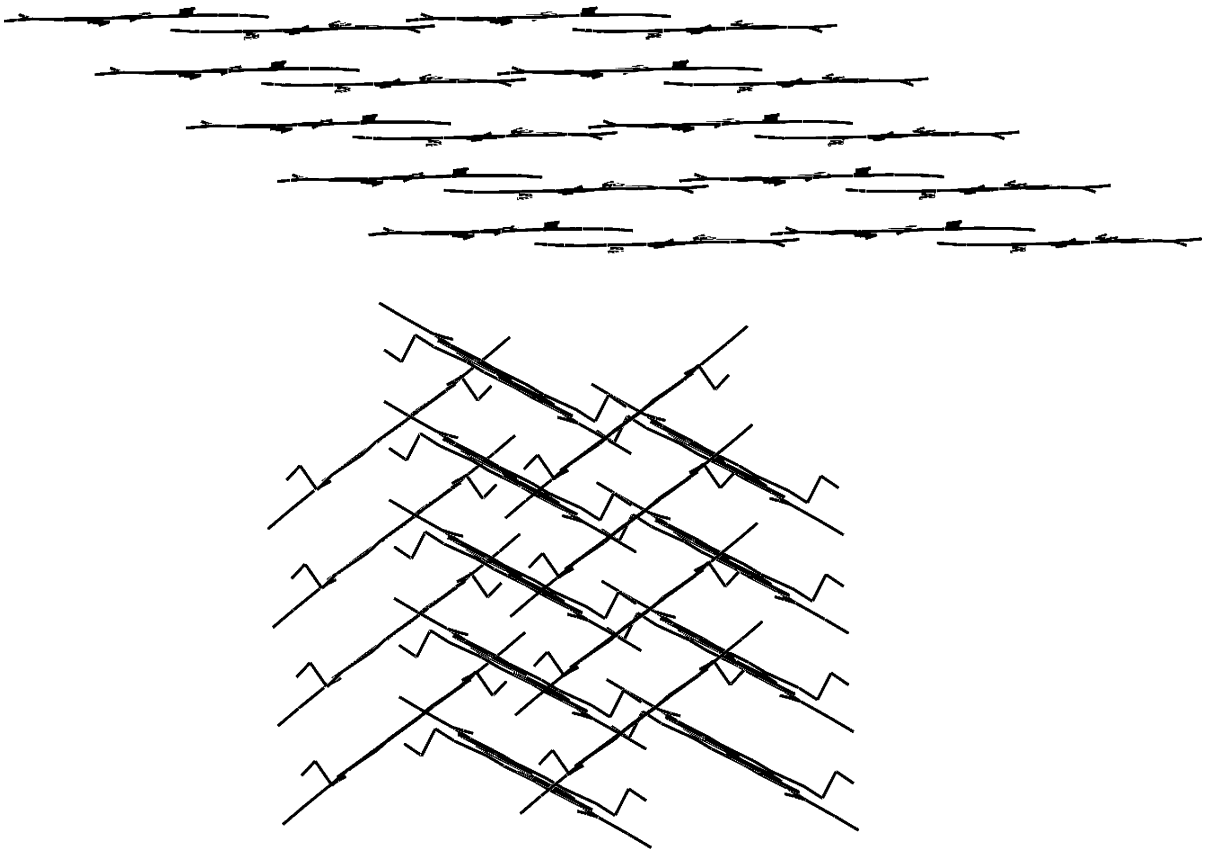

Figure 6. Packing diagrams showing the layered packing of **Q3** (upper) and the layered herringbone packing of **Q4** (lower).

Table 3. Comparison of Selected Structural Data and Calculations

compound	π-stacking distances (Å)	area overlap (%)	volume overlap (Å³)	C_K[a]	HOMO splitting[b] (meV)	LUMO splitting[b] (meV)
Q1	3.335	13.5	3.28	0.709	c	c
	3.455	71.0	14.1		c	c
Q2	3.393	56.0	13.0	0.696	204	353
Q3	3.492	44.8	8.78	0.682	147	219
Q3tol	3.404	4.8	1.10	0.682	c	c
	3.465	26.5	5.50			
Q4	3.358	65.5	21.3	0.724	317	417
DCMT	3.456	73.3	16.0	0.685	c	c
	3.650	37.5	5.3		c	c

[a] Kitaigorodskii packing coefficient. [b] Calculated from the crystallographic atom positions for a dimer. [c] Not calculated.

and Gavezotti[36] define four distinct crystal-packing arrangements for aromatic hydrocarbons. Pentacene falls into the herringbone motif where nearest neighbors are not parallel. The β motif with a layered structure of parallel nearest neighbors describes the packing of **Q1**, **Q2**, **Q3**, and **Q3tol**. **Q4** and **DCMT** exhibit the γ motif, which is a type of flattened out herringbone structure with parallel nearest neighbors but with more than one orientation of layers. (An additional aromatic hydrocarbon motif previously described (sandwich motif) is not observed in any of the structures to be discussed here.) In the structures of **Q2**, **Q3**, and **Q4**, a single unique π-stacking distance is observed, and the molecules in adjacent layers (Figure 5) pack in a parallel arrangement with the corresponding thiophene rings pointing in the same direction as the layers above and below a given molecule. The structures of **Q3tol**, **Q1**, and **DCMT** exhibit dimer motifs (Figure 4) with two unique stacking distances. The molecules in the stack alternate in an antiparallel fashion with analogous thiophene rings pointing in the direction opposite to that of molecules in adjacent layers. The antiparallel stacking seems to be intimately related to the formation of dimers in these structures. An additional difference between the dimer structures and those with only one stacking distance is that the dimer structures exhibit an oscillation of the pitch angle between adjacent layers (pitch angle alternates between positive and negative from the perpendicular stacking vector). This sawtooth pattern is different from the stair-step pattern of the single-distance stacking structures, in which the unique pitch angle displaces the stack the same direction along the length of the molecule.

The extreme flatness enforced by the quinoidal bonding motif common to all of the molecules allows for very short $\pi-\pi$ stacking distances and significant π-overlap of adjacent molecules within a stack. The closest observed stacking distances in these molecules range from 3.335 Å in **Q1** to 3.492 Å in **Q3**. The observed stacking distances in these structures are almost all shorter than the previously determined **DCMT** structure (3.456 and 3.650 Å). The stacking distances (shown in Table 3) are very short relative to the few nonquinoidal thiophene structures with π-stacking. For example, NC-3T-CN (2,2′:5′,2″-terthiophene-5,5″-dicarbonitrile)[37] stacks with $\pi-\pi$ distances of 3.65−3.70 Å; Me$_2$*t*-BuSi-3T-Me$_2$*t*-BuSi (5,5″-bis(*tert*-butyldimethylsilyl)-2,2′:5′,2″-terthiophene)[38] stacks with a

(36) Desiraju, G. R.; Gavezotti, A. *Acta Crystallogr*. **1989**, *B45*, 473−482.

(37) Barclay, T. M.; Cordes, A. W.; MacKinnon, C. D.; Oakley, R. T. Reed, R. W. *Chem. Mater*. **1997**, *9*, 981−990.

(38) Barbarella, G.; Ostoja, P.; Maccagnani, P.; Pudova, O.; Antolini, L.; Casarini, D.; Bongini, A. *Chem. Mater*. **1998**, *10*, 3683−3689.

$\pi-\pi$ distance of 3.98 Å, and NO_2-(3TBu_2)-NO_2 (3′,4′-di-*n*-butyl-5,5″-dinitro-2,2′:5′,2″-terthiophene)[16] stacks as a dimer with one short distance (3.556 Å) and a longer distance (3.573 Å). Recently, tricyanovinyl-substituted terthiophenes[39,40] have also been shown to π-stack with distances of 3.535 and 3.528 Å for π-dimers in TCV-terthiophene (5-(tricyanovinyl)-2,2′:5′,2″-terthiophene)[39] and 3.552 and 3.544 Å for π-dimers in TCV-(3TBu_2)-TCV (3′,4′-di-*n*-butyl-5,5″-di(tricyanovinyl)-2,2′:5′,2″-terthiophene).[40] A related heterosoric charge-transfer complex bithiophene-TCNQ (2,2′-bithiophene tetracyanoquinodimethane)[41] has a unique stacking distance of about 3.37 Å with an almost parallel stacking motif (1.2° between adjacent planes). The low-temperature crystal structure of [Ph-(3TBu_2)-Ph][PF_6] (3,4′-di-*n*-butyl-5,5″-diphenyl-2,2′:5′,2″-terthiophene hexafluorophosphate)[19] has short π-stacking distances of 3.358 and 3.433 Å. Finally, for comparison, the interplanar spacing in graphite is 3.35 Å,[42] roughly equal to the sum of the van der Waals thickness of adjacent layers.

These comparisons suggest that the short π-stacking distances observed in these quinoidal thiophenes are more similar to those found in charge-transfer complexes or the oxidized terthiophene structures than to nonquinoidal terthiophene structures.[1,15] The donor−acceptor roles are predetermined in CT complexation of two component systems. In the oxidized terthiophene structures, the strong interactions between adjacent molecules occur through π-dimerization of odd electron radical species. In the structures **Q1**−**Q4**, the low reduction and oxidation potentials of these molecules allow each molecule to simultaneously assume donor and acceptor properties. Additionally, in the structure of the **Q3** toluene solvate (**Q3tol**), two-component donor−acceptor interactions are evident as toluene functions as an additional donor in the π-stacking of **Q3** molecules.

An interesting question is whether the π-stacking distance correlates with the extent of π-overlap with adjacent molecules or if the other packing forces determine the distance and hence the overlap. Combining the pitch and roll distances with a rectangular approximation of the molecular plane and π-system of each molecule allows the projected area overlaps of molecules in adjacent planes to be measured (Table 3). Inspection of the area overlap versus π-stacking distance plot (Figure 7) reveals a linear correlation between overlap and distance for **Q4**, **Q2**, and **Q3**. However, for the dimerized structures, the better area overlap does not always correlate with shorter $\pi-\pi$ distances. In the cases of **Q1** and **Q3tol**, the longer inter-dimer stacking distance has better parallel area overlap, while **DCMT** shows the opposite behavior. In the three structures with only one π-stacking distance, the shorter distance correlates with a larger area overlap (Figures 5, 7), and we conclude that the π-area overlap is correlated with the π-stacking distance in a simple way for only the single distance structures.

A second way to compare the extent and magnitude of intermolecular π-interactions along the stacking axis is to take into account a "π-volume overlap". A π-volume overlap between the π-systems of adjacent molecules is a better comparison because it takes into account not only the slip of the π-system, but also the stacking distance. The geometric volume overlap considered here is the difference between 4 Å (an arbitrary distance chosen for zero $\pi-\pi$ interaction) minus the π-stacking distance between adjacent molecules multiplied by the area overlap. Calculated π-volume overlaps are shown in Table 3. The **DCMT** compound that we have already studied and shown to have relatively good electron mobility and a significant hole mobility is typical of the series. Of importance is the significantly larger value of this parameter for **Q4**, which clearly has the best volume π-overlap in the series. Curiously, pentacene has a π-overlap volume of zero, because there is no parallel area overlap of the π-system in the structure. Although these area and volume overlap comparisons are based on only geometric considerations and do not take into account atomic overlaps between carbon p-orbitals, we believe they will have predictive value because they allow direct structural comparisons of various polythiophene oligomers. In a later section of this paper, we will show the correlation of the area and volume overlap parameter with the more rigorous bandwidth calculations based on molecular orbital calculations.

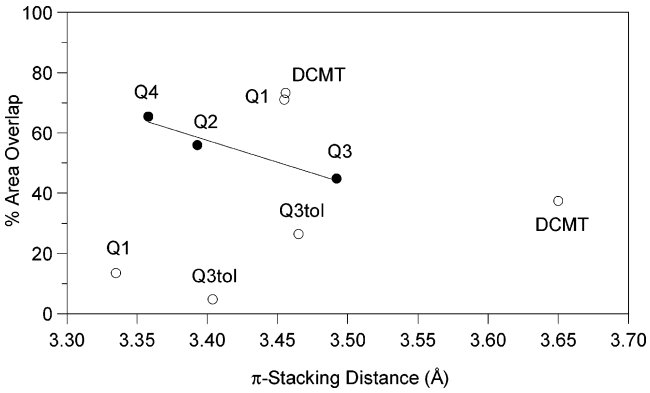

Figure 7. Area overlap versus π-stacking distance comparison. The solid line indicates the three molecules with one unique stacking distance.

As the overall packing structure of these molecules is determined by maximizing the contributions of the most important molecular interactions, the intermolecular interactions in the directions roughly perpendicular to the stacking axes have been investigated. Nitriles have been shown to exert supramolecular organization in compounds with halogens, chalcogens, and C−H groups including thiophenes.[37,43] Pairwise interactions between nitrile groups and polarizable thiophene hydrogens appear frequently in structures of **Q1**−**Q4**. We suggest that these interactions are the important determiners of the geometry within the layers, which, in turn, adjust interlayer steric interactions. Thus, the π-stacking distance and the extent of slippage in the pitch and roll angles are both affected, but not in a simple way. A summary of the geometry and distances of these nitrile−thiophene hydrogen interactions is given in Table 4. In **Q1**, each molecule has two unique pairwise nitrile−thiophene hydrogen interactions (N1−H5A, N4−H10A), utilizing an end-ring hydrogen in one interaction and a center-ring hydrogen in the

(39) Bader, M. M.; Custelcean, R.; Ward, M. D. *Chem. Mater*. **2003**, *15*, 616−618.
(40) Pappenfus, T. M.; Burand, M. W.; Janzen, D. E.; Mann, K. R. *Org. Lett*. **2003**, *5*, 1535−1538.
(41) Minxie, Q.; Heng, F.; Yong, C. *Jiegou Huaxue (Chinese J. Struct. Chem.)* **1986**, 159.
(42) Cotton, F. A.; Wilkinson, G. *Advanced Inorganic Chemistry*, 5th ed.; Wiley: New York, 1988.
(43) (a) Reddy, D. S.; Ovchinnikov, Y. E.; Shishkin, O. V.; Struchkov, Y. T.; Desiraju, G. R. *J. Am. Chem. Soc*. **1996**, *118*, 4085−4089. (b) Cordes, A. W.; Haddon, R. C.; Hicks, R. G.; Oakley, R. T.; Palstra, T. T. M. *Inorg. Chem*. **1992**, *31*, 1802−1808. (c) Cordes, A. W.; Haddon, R. C.; Hicks, R. G.; Kennepohl, D. K.; Oakley, R. T.; Palstra, T. T. M.; Schneemeyer, L. F.; Scott, S. R.; Waszczak, J. V. *Chem. Mater*. **1993**, *5*, 820−825.

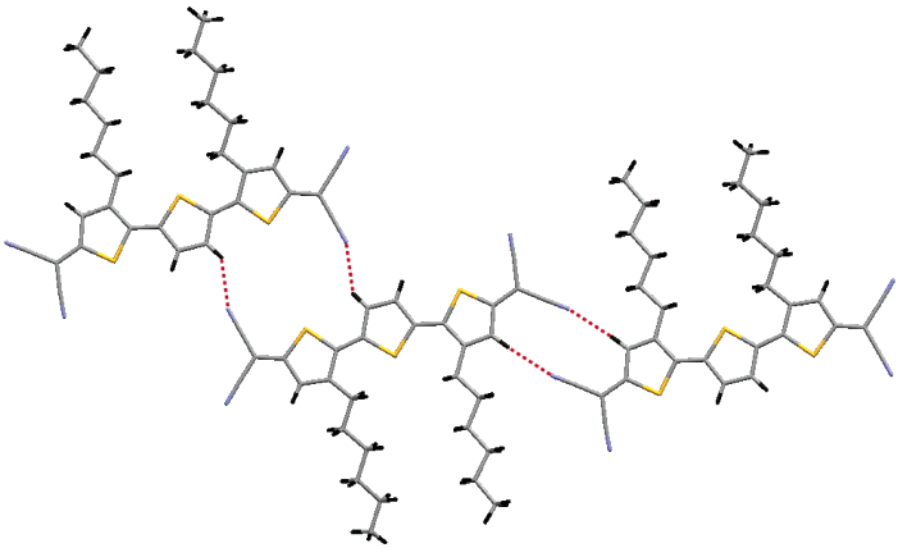

Figure 8. Intermolecular thiophene hydrogen−nitrile interactions in the structure of **Q1**.

Table 4. Summary of Distances and Geometry of Nitrile−Thiophene Hydrogen Interactions

compound	donor atom	acceptor atom	distance (Å)	distance − VDW[a] (Å)	CH–N angle (deg)	CN–H angle (deg)
Q1	N1	H5A	2.538	−0.212	169.2	163.9
Q1	N4	H10A	2.539	−0.211	139.7	157.3
Q2	N3	H14A	2.541	−0.209	175.5	169.2
Q3	N1	H5A	2.866	0.116	173.2	168.5
Q3tol	N2	H9A	2.716	−0.034	169.0	157.6
Q4	N2	H10A	2.597	−0.153	148.0	115.8

[a] VDW is the sum of the van der Waals radii of the donor and acceptor atoms.

other. Figure 8 shows the nitrile−thiophene hydrogen interactions of **Q1**. **Q2** only has one nitrile end-ring thiophene hydrogen interaction (N3−H14A). **Q3** has a similar interaction at a longer distance (N1−H5A). **Q3tol** has a middle-ring hydrogen interaction with a nitrile (N2−H9A). **Q4** has an inner-ring hydrogen interaction (N2−H10A). In **DCMT**, interactions between nitrile groups and thiophene hydrogens are present, but they occur between molecules in π-stacks that are not parallel.

Although the nitrile−thiophene hydrogen interactions are important intermolecular interactions for packing determination, additional intermolecular interactions evidenced by close contacts were discovered. Only those contacts with reasonable geometry considerations are noted here. Close parallel nitriles are present in a plane of the structure of **Q2** (C1−N1) and are only 3.173 Å apart. A close S1−H30D approach of 2.817 Å is present in the structure of **Q1**. A close S2−N2 distance of 3.304 Å is found in the structure of **Q4**. In all structures, there are no S−thiophene hydrogen interactions. Numerous close contacts also exist between alkyl groups in each structure. While association of the alkyl chains occurs in all of these structures, these interactions are considered to be weak in comparison with the forces driving π-stacking and the nonclassical hydrogen bonding of the nitriles.

Bandwidth Calculations. Parallel area overlap calculations approximate the interaction between adjacent molecules but do not capture the shape of the molecular orbitals;[44] however, MO calculations that are described below show that the area overlap correctly predicts the order of the electronic coupling in the π-stacks for the single distance structures considered here. Detailed MO calculations were performed to understand the intermolecular interactions in the solid-state structures of the quinoidal oligothiophenes in this study. The calculations also provide a means of comparing existing calculations of molecular structures for which TFT devices have been constructed. Calculations were performed only on the structures with one unique π-stacking distance as the dimer structures represent a different type of intermolecular interaction between adjacent molecules. The methodology used to explore nearest-neighbor interactions involved the calculation of the HOMO−LUMO band splittings of a molecule and each neighbor in the experimentally determined X-ray structure to a distance where interactions were negligible. One way to quantify the electronic coupling between adjacent molecules has been defined as the transfer integral (t), which is approximately one-half the HOMO/HOMO and LUMO/LUMO splittings for a dimer and is different for the HOMO and the LUMO. Bandwidths for both the HOMO and the LUMO in an extended one-dimensional stack are $4t$ according to the tight binding approximation.[45]

For the case of **Q4**, the only significant interactions calculated were between adjacent molecules within a π-stack. Using the tight binding approximation, we can approximate the bandwidths of an infinite stack for the HOMO as 633 meV and the LUMO as 834 meV. The evolution of the bandwidth as a function of the number of molecular units in a π-stack linearly correlates with the function $\cos(\pi/(N+1))$ (where N = number of interacting oligomers in the cluster), which validates the use of the tight binding approximation (Figure 9). For comparison, similar calculations for bisdithienothiophene (BDT),[46] which packs in a γ motif with a π-stacking distance of 3.557 Å but exhibits a large roll distortion which causes poor area overlap, have given HOMO and LUMO bandwidths of 688 and 108 meV, respectively. BDT only has significant HOMO−LUMO splittings along the π-stacking direction. Bandwidth calculations of pentacene,[46] which packs in a herringbone motif with no

(44) Kazmaier, P. M.; Hoffman, R. *J. Am. Chem. Soc.* **1994**, *116*, 9684−9691.

(45) Brédas, J.-L.; Calbert, J. P.; da Silva Filho, D. A.; Cornil, J. *Proc. Natl. Acad. Sci. U.S.A.* **2002**, *99*, 5804−5809.

(46) Cornil, J.; Calbert, J. P.; Beljonne, D.; Silbey, R.; Brédas, J.-L. *Adv. Mater.* **2000**, *12*, 978−983.

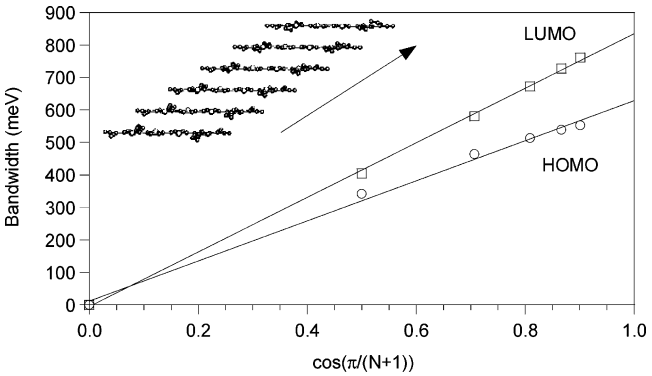

Figure 9. Calculated bandwidth evolution of **Q4**. Cluster size increases to the right.

obvious π-stacking, but with significant edge-to-face interactions, indicate significant transfer integrals in two different directions, yielding two-dimensional electronic coupling character. The total HOMO and LUMO bandwidths calculated are 608 and 588 meV, respectively. Although the **Q4** calculation shows distinctly one-dimensional charge transport character (along the π-stack), the HOMO bandwidth calculated for **Q4** is similar to that of pentacene and the LUMO bandwidth is considerably larger.

In the case of **Q2** and **Q3**, the strongest pairwise interactions are again between adjacent molecules within a π-stack, but significant interactions were also found beyond nearest neighbors within a π-stack and for some of the nearest neighbors in adjacent π-stacks. Particularly in the case of **Q3**, the parallel stacking of molecules in a given π-stack causes the alignment of the large (6.5 D, according to an INDO calculation) molecular dipole moments for all molecules in the stack. These longer-range dipole−dipole interactions cause a breakdown of the nearest-neighbor approximation. When a dimer is extracted from the crystal structure to compute the orbital splittings, the two molecules in the dimer will no longer be equivalent. In this case, the HOMO−LUMO splittings do not simply correspond to twice the transfer integral;[33,47] as a result, we do not provide bandwidths for **Q2** and **Q3**.

The HOMO−LUMO splittings ($2t$) calculated for dimers in the **Q2**, **Q3**, and **Q4** structures allow a comparison of the intermolecular interaction between adjacent molecules in the solid state; the values are summarized in Table 3. The largest HOMO−LUMO splittings are observed for **Q4**, with **Q2** as next largest. It is interesting to note that for this series the stacking distances, area overlaps, and calculated band splittings are consistent with one another.

(47) Senthilkumar, K.; Grozema, F. C.; Bickelhaupt, F. M.; Siebbeles, L. D. A. *J. Chem. Phys.* **2003**, *119*, 9809−9817.

Conclusions

The synthesis and characterization of quinodimethane-substituted oligomers are reported. The electrochemistry of these materials indicates their suitability for both p and n biasing in FETs. The structural features of these materials are favorable for efficient transport. Together, these features indicate **DCMT** derivatives are good candidates for ambipolar semiconductor materials. Preliminary evidence supports this conclusion.[11] Close π-stacking, large area overlap, and significant intermolecular electronic coupling, as calculations indicate, correlate for structures with a unique π-stacking distance and parallel cofacial arrangement. Calculations suggest that these compounds could exhibit hole and electron mobilities in devices that could rival those of pentacene if the proper thin film morphology and other important device parameters are also favorable.

Acknowledgment. This work was supported primarily by the MRSEC Program of the National Science Foundation under Award Number DMR-0212302. P.C.E. would like to acknowledge Professor Larry Miller for the generous donation of his lab space and many helpful discussions. D.E.J. would like to acknowledge the University of Minnesota Department of Chemistry for financial support through a Block Grant Fellowship as well as the University of Minnesota Graduate School for support through a Doctoral Dissertation Research Grant. We would like to acknowledge the X-ray crystallographic laboratory in the University of Minnesota Department of Chemistry. ChemMatCARS Sector 15 is principally supported by the National Science Foundation/Department of Energy under grant number CHE0087817 and by the Illinois board of higher education. The Advanced Photon Source is supported by the U.S. Department of Energy, Basic Energy Sciences, Office of Science, under Contract No. W-31-109-Eng-38.

Supporting Information Available: ORTEP diagrams and crystallographic data in CIF format. This material is available free of charge via the Internet at http://pubs.acs.org.

JA0484597